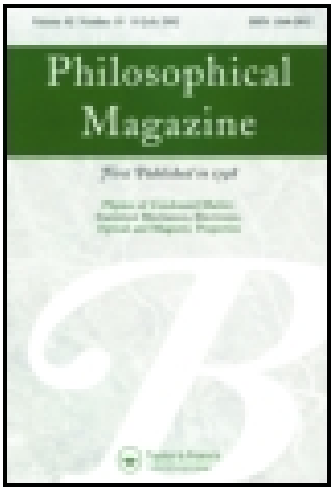

Philosophical Magazine Part B
Publication details, including instructions for authors and subscription information:
http://www.tandfonline.com/loi/tphb20

Kink-kink interactions and pre-roughening of vicinal surfaces

Santi Prestipino [a b] & Erio Tosatti [a b c]
[a] Istituto Nazionale per la Fisica della Materia , Italy
[b] International School for Advanced Studies , Trieste, Italy
[c] International Centre for Theoretical Physics , Trieste, Italy
Published online: 25 Aug 2009.

To cite this article: Santi Prestipino & Erio Tosatti (2001) Kink-kink interactions and pre-roughening of vicinal surfaces, Philosophical Magazine Part B, 81:7, 637-674, DOI: 10.1080/13642810108205769

To link to this article: http://dx.doi.org/10.1080/13642810108205769

PHILOSOPHICAL MAGAZINE B, 2001, VOL. 81, NO. 7, 637–674

Kink–kink interactions and pre-roughening of vicinal surfaces

SANTI PRESTIPINO†‡|| and ERIO TOSATTI†‡§¶

† Istituto Nazionale per la Fisica della Materia,
‡ International School for Advanced Studies, Trieste, Italy
§ International Centre for Theoretical Physics, Trieste, Italy

[*Received 29 January 2001 and accepted 21 February 2001*]

ABSTRACT

Thermal anisotropic roughening of vicinal surfaces is well known and well studied. Here, we consider the possibility that a separate pre-roughening transition might take place, prior to roughening. Within the framework of a terrace–step–kink model, we identify possible interaction mechanisms for promoting pre-roughening (PR) and the ensuing disordered flat (DOF) phase. In particular, the most likely to occur in real systems is a short-range repulsion between equally oriented parallel kinks. When this interaction is strong, PR shows up and the DOF phase is characterized by antiparallel order of kinks within a step. Next, we discuss the relevance of this scenario for real vicinals, in particular Ag(115), where high-accuracy scanning tunnelling microscopy data are available.

§ 1. INTRODUCTION

Stepped surfaces of metals have recently attracted much interest, both theoretically and experimentally, as they provide a valuable tool for investigating the interaction and dynamics of various types of defect on a surface, including steps, kinks and adatoms. In particular, the presence of steps already at zero temperature makes it possible for a vicinal surface, that is a surface consisting of a regular array of terraces, to roughen at a much lower temperature than the melting temperature (Villain *et al.* 1985). This leads to a complete decoupling of the two phenomena of melting and roughening and allows for a neat observation of surface roughening through the use of scanning tunnelling microscopy (STM), such as recently reported for Ag(115) (Hoogeman *et al.* 1996, 1999, Hoogeman and Frenken 2000). In fact, any vicinal surface would be rough down to $T = 0$ if the steps did not repel each other. However, the elastic distortions which appear in the neighbourhood of any surface defect provide an ubiquitous source of repulsion between the steps. Together with the entropy gained from the enhanced vibration of step particles, this elastic repulsion is held responsible for the thermodynamic stability of vicinal surfaces at all but the very low temperatures where they could simply be metastable (Frenken and Stoltze 1999).

|| Author for correspondence. Email: prestip@sissa.it
¶ Email: tosatti@sissa.it

Philosophical Magazine B ISSN 1364–2812 print/ISSN 1463–6417 online © 2001 Taylor & Francis Ltd
http://www.tandf.co.uk/journals
DOI: 10.1080/13642810110050567

Across the roughening transition, a macroscopic change is observed in the morphology of the vicinal. Below the roughening temperature T_R, steps remain sufficiently ordered. Above T_R, steps meander freely and kinks abound (a kink is a step in the step), giving rise to divergent fluctuations in the position of the surface height profile. However, the roughening behaviour can be more complex if kinks are taken to interact. In particular, we know from elasticity theory that a repulsive interaction should be expected between two identical kinks at distance r on a step (parallel kinks), which asymptotically decays as r^{-3} (Marchenko and Parshin 1981, Rickman and Srolovitz 1993). If this repulsion is strong enough, it could be possible to stabilize a disordered flat (DOF) phase, characterized by strong antiparallel correlations between consecutive kinks in the same step. This phase would be disordered in that kinks are present in a large amount along the steps, but flat, because of the limited step lateral excursion. A new phase transition would occur in this case, called pre-roughening (PR) in similar contexts (Den Nijs and Rommelse 1989), whereas roughening would be shifted at a higher temperature.

In this paper, we investigate this possibility through a specific model, and find that promotion of a DOF phase by kink–kink repulsion is indeed possible. This is an important result, since it shows that a vicinal surface can exist in a phase that was never considered before. Moreover, even in the absence of any interaction between the kinks, a DOF phase could nonetheless be stabilized by a sufficiently strong and long-range step–step repulsion.

A PR transition is strongly believed (Den Nijs 1991, Weichman and Prasad 1996. Jagla *et al.* 1999, Prestipino and Tosatti 1999, Celestini *et al.* 2000) to underlie the well-documented re-entrant layering observed on the (111) surface of rare-gas solids (Youn and Hess 1990, Day *et al.* 1993, Youn *et al.* 1993). The deconstruction transition of some metal surfaces such as Au(110) can also be regarded as a realization, although less interesting, of PR. It is still an open issue whether a stable DOF phase is present in an unreconstructed metal surface, although the possibility of a DOF phase separation has also been envisaged in this case (Prestipino and Tosatti 1998). In particular, it is possible that the incomplete melting observed on Pb(100) and on Au(100) could be accompanied by PR. With our emphasis on the vicinal DOF phase, we wish to draw the attention of experimentalists towards a new class of metal surfaces where a concrete realization of PR could be found.

Our suggested PR of vicinals is general. However, owing to the excellent characterization of one particular vicinal, Ag(115), provided by Hoogeman *et al.* (1996, 1999) and Hoogeman and Frenken (2000), we shall specialize the quantitative aspects of our study to that surface. Hoogeman and co-workers have addressed the problem of roughening of Ag(115) through the measurement of a kink–kink correlation function which is found to level off at large distance below T_R, while being logarithmically divergent as a function of surface size above T_R. However, an inconsistency is found in that study between the thermal behaviour of the pre-factor of the kink–kink correlation function and the correlation length. While the former indicates roughening at around 490 K, the correlation length points to a divergence at a lower temperature (about 440 K). Accepting the reported accuracy on the correlation length, a possible way out could be the existence of a DOF phase in the interval 440–490 K. In the light of this possibility, it is of interest to reconsider the nature of the phase transition observed in Ag(115), trying to see whether a new, possibly more accurate schematization of it (with parameters extracted from the experiment) gives support to the view of a single roughening transition around

430 K (Hoogeman *et al.* 1999, Hoogeman and Frenken 2000) or, rather, reveals a more complicated scenario, with both PR and roughening.

This paper is organized as follows. In § 2, we introduce a modified terrace–step–kink (MTSK) model for the fcc (115) surface. Our model is a generalization of the standard Villain–Grempel–Lapujoulade (VGL) model, where interactions between the kinks are also taken into account. Next § 3 is an intermezzo, devoted to seeking an analytic solution of a modified VGL model where an extended step–step repulsion acts as a mechanism for promoting the DOF phase. In § 4, the results of a Monte Carlo simulation of the MTSK model are analysed, confirming the existence of PR for strong enough kink–kink repulsion. Then § 5 is devoted to an attempt to fit the MTSK model to Ag(115). With this aim, one could in principle use atomistic potentials to estimate the MTSK parameters. However, kink–kink interactions are generally given as differences in the step energies, which are in turn very difficult to obtain accurately by numerical studies of crude models such as the embedded-atom method. Therefore, we shall only tackle the question of whether, within the MTSK model, the incomplete information available from the STM experiment is compatible with the existence of the DOF phase. Further comments and conclusions are offered in § 6.

§ 2. A TERRACE–STEP–KINK MODEL WITH INTERACTING KINKS

An ideal high-index (vicinal) surface consists of terraces of a low-index facet, separated by straight steps running along a direction of strong bonding. In this paper, we consider a fcc metal (115) surface as a specific example (figure 1), having in mind the case when the fcc metal is Ag. This vicinal is formed by (001) terraces of

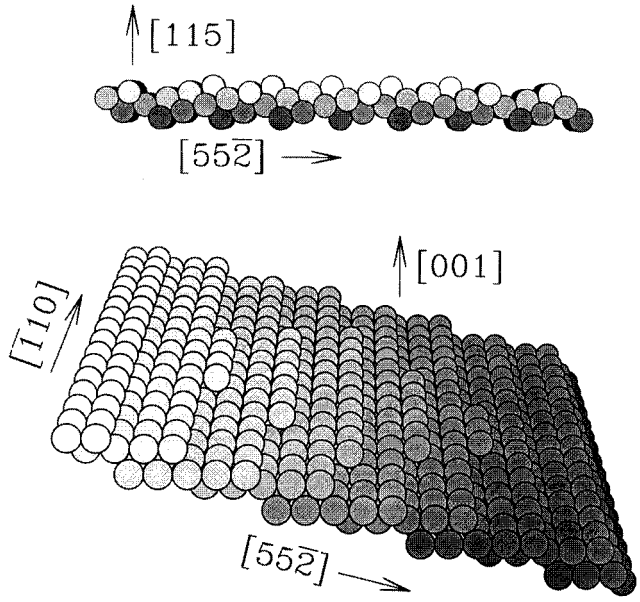

Figure 1. A small portion of a fcc metal (115) surface is shown with a terrace above, delimited by a secondary step formed by kinks along the primary (111) steps. It can be appreciated from the side view that, owing to the terrace, the height of the surface along its normal [115] direction becomes increased by a fraction $\sin\alpha = 6^{1/2}/9$ of the lattice parameter a, α being the mean slope of the vicinal over the x–y plane.

width $2.5a$, where a is the distance between nearest-neighbour atoms in the fcc lattice ($a \approx 2.9$ Å for Ag). Two adjacent terraces are separated by a (111) (primary) step. Other steps are formed by kinks along primary steps (they are called secondary steps); proliferation of secondary steps is responsible for vicinal roughening. Upon moving from one terrace to the next, all atomic positions at the surface become displaced by $a/2$ along the x and y directions; this allows identification of two different square sublattices on this plane. Finally, the normal direction to the surface forms an angle α of 15.8° with respect to the vertical [001] direction; this angle α is the average slope of the vicinal over the x–y plane.

We are interested in describing the thermal disordering of the fcc metal (115) surface. However, we do not want to consider the high-temperature melting behaviour of the vicinal or even approach the roughening temperature of the (001) facet (since the melting temperature is much greater, there is no room here for an interplay between PR and surface melting of the type investigated by Jagla *et al.* (1999), which, above T_{PR}, would rather require a description in terms of continuous degrees of freedom). In such a low-temperature regime, a good approximation is to exclude the possibility of adatoms (i.e. poorly coordinated particles) on terraces; in this case, the only relevant variables that are left in the problem are the step positions. We assume that migration of step atoms across the boundaries of a selected surface region acts to maintain full grand-canonical conditions inside this region. Finally, a solid-on-solid condition is assumed to hold over all the step length, in such a way that, taking the y axis in the direction of steps at $T = 0$, the step position with respect to $T = 0$ can be encoded by a variable $u_m(y)$ ($m = 1, \ldots, N_x$ being the step label and $y = 1, \ldots, N_y$ the abscissa along the step).

This so-called terrace–step–kink (TSK) model is very old (Kossel 1927, Stranski 1928). It assumes some sort of repulsion between neighbouring steps and an energy cost for forming kinks along the steps. This model has the advantage of being simple enough and also amenable in some cases to an exact statistical treatment; yet, it gives an accurate description of the roughening transition in vicinals.

A particular TSK model was introduced for this problem by VGL. In their model, y and $u_m(y)$ are both integers and the difference between $u_m(y+1)$ and $u_m(y)$ is restricted to 0, ±1 (i.e. only kinks of unitary length are permitted). The Hamiltonian of the VGL model (which is in fact specific to the sc (001) vicinal surfaces) is

$$H = W_1 \sum_{m,y} [u_m(y+1) - u_m(y)]^2 + \sum_{m,y} f(u_{m+1}(y) - u_m(y)), \tag{1}$$

with

$$f(\Delta u) = \begin{cases} 0 & \text{for } \Delta u \geqslant 0, \\ U_1 & \text{for } \Delta u = -1, \\ +\infty & \text{for } \Delta u < -1. \end{cases} \tag{2}$$

With two parameters only, W_1 and U_1, the Hamiltonian (1) is only appropriate for step densities which are not too low, where $u_{m+1}(y)$ is strongly disfavoured by the small terrace width from being smaller than $u_m(y) - 1$. $W_1 > 0$ is the kink formation energy, while $U_1 > 0$ accounts for a short-range repulsion between the steps. Periodic boundary conditions (PBCs) are meant to hold in the x direction in order

to prevent the step array from 'evaporating' (i.e. conservation of the step number in any given sample is always implied). PBCs are also applied in the y direction.

Model (1) is exactly solvable in the large-anisotropy $W_1/U_1 \to +\infty$ limit, corresponding to an infinite bond strength in the y direction (Villain *et al.* 1985). In this limit, the Hamiltonian (1) can be mapped on to a well-studied one-dimensional (1D) quantum spin problem (see § 3). In particular, a Kosterlitz–Thouless phase transition is predicted to occur at a temperature T_R given by

$$\frac{U_1}{2k_B T_R} \exp\left(\frac{W_1}{k_B T_R}\right) = 1. \tag{3}$$

This transition is interpreted as surface roughening in that the correlation function

$$G(m) = \langle [u_m(y) - u_0(y)]^2 \rangle \tag{4}$$

is bounded from above as m goes to infinity when $T < T_R$, while it diverges logarithmically in the same limit when $T > T_R$. Above T_R, owing to proliferation of thermally excited kinks, steps are no longer confined near $u = 0$ and the mean surface slope becomes undefined.

We have modified the Hamiltonian (1) by including terms which represent interactions between the kinks. These interactions generally arise from the mutual interference of the elastic strain fields as determined by the individual kinks. In particular, we allow for a short-range repulsion between parallel kinks in the same step and also between parallel kinks in neighbouring steps. Instead, no interaction will be assumed between antiparallel kinks. Finally, the number of atomic positions along the y axis has been doubled, so as to take into account the two-sublattice structure of the fcc (115) surface (figure 2). As a result, the restriction to unitary kinks now reads as $u_m(y+2) - u_m(y) = 0, \pm 1$. With the further prescription that y values are, say, odd for m odd, and even for m even, our MTSK Hamiltonian looks as follows:

$$\begin{aligned} H = {} & W_1 \sum_{m,y} \delta[|u_m(y+2) - u_m(y)| - 1] \\ & + W_2 \sum_{m,y} \delta[|u_m(y+4) - u_m(y)| - 2] \\ & + W_3 \sum_{m,y} \delta[|u_m(y+6) - u_m(y)| - 2] \\ & + \sum_{m,y} [f_1(u_{m+1}(y) - u_m(y-1)) + f_1(u_{m+1}(y) - u_m(y+1))] \\ & + \sum_{m,y} [f_2(u_{m+1}(y) - u_m(y-3)) + f_2(u_{m+1}(y) - u_m(y+3))], \end{aligned} \tag{5}$$

where f_1 and f_2 are defined as

$$f_1(\Delta u) = \begin{cases} 0 & \text{for } \Delta u > -1, \\ U_1 & \text{for } \Delta u = -1, \\ +\infty & \text{for } \Delta u < -1, \end{cases}$$

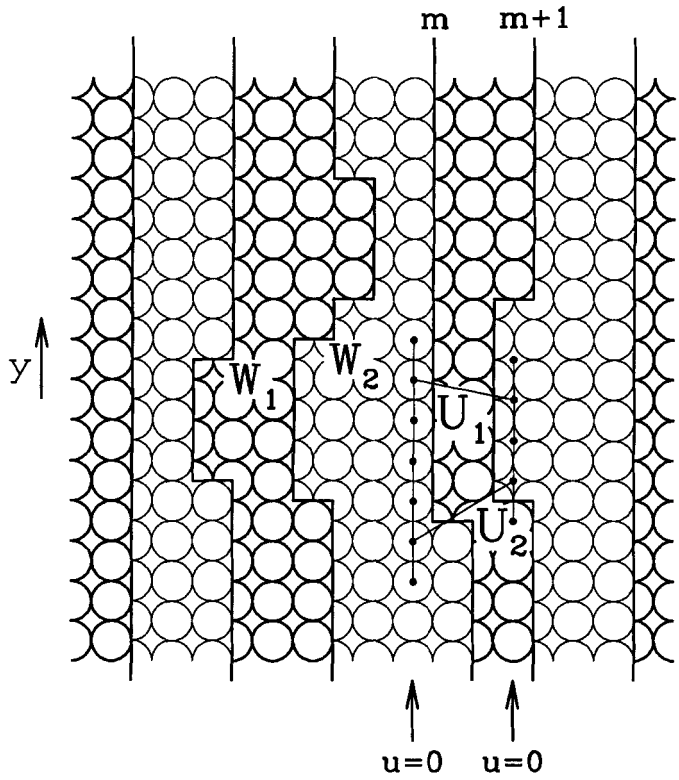

Figure 2. Schematic view of the MTSK surface, with a number of permitted excitations and their energy cost. Atomic positions along a step are all even or all odd according to which sublattice the terrace atoms on the left of the step belong to.

$$f_2(\Delta u) = \begin{cases} 0 & \text{for } \Delta u > -2, \\ U_2 & \text{for } \Delta u = -2, \\ +\infty & \text{for } \Delta u < -2. \end{cases} \tag{6}$$

In equation (5), m runs from 1 to N_x, y takes (depending on the parity of m) either the odd or the even values from 1 to $2N_y$, $\delta(\ldots)$ is the Kronecker function and all parameters are positive. In particular, W_2 and W_3 discourage parallel kinks from occurring at first- or second-neighbour positions on the same step, while U_2 represents a short-range repulsion between parallel kinks in neighbouring steps. Within this set-up, we expect that a strong kink–kink repulsion could induce a DOF phase into the MTSK model (see § 4).

Even if kinks were non-interacting, $U_2 = W_2 = W_3 = 0$, the DOF phase could nevertheless be favoured by a suitably long-ranged step–step repulsion which may encourage step localization without discouraging kink proliferation. However, repulsive forces between the steps decay as r^{-2} at large distance (Marchenko and Parshin 1981, Rickman and Srolovitz 1993). When a step is displaced from its reference position, the excess interaction energy at distance r approximately changes by $(r+1)^{-2} + (r-1)^{-2} - 2r^{-2} \approx r^{-4}$; this means that the (excess) step–step repulsion is heavily suppressed at large distances. For this reason, we believe that kink–kink repulsion is the only relevant mechanism for the appearance of the DOF phase in a

vicinal. In spite of this, the effect of a longer-range step–step repulsion on the phase diagram of the VGL model is worth considering anyway, and it is moreover amenable to an analytic treatment. This is the subject of the next section.

§ 3. Extended step–step repulsion in the Villain–Grempel–Lapujoulade model

The Hamiltonian (1) was designed in such a way as to be equivalent, in the large-ansiotropy limit, to a solvable 1D quantum problem (the spin-$\frac{1}{2}$ Heisenberg antiferromagnetic (AFM) Ising chain) (Villain *et al.* 1985). This isomorphism rests ultimately on the equivalence between the partition function of the original model and the imaginary-time propagator of a suitable quantum system with one less space dimension (Hertz 1976). In particular, the free energy of the statistical model is simply proportional to the ground-state energy of the quantum model; as a result, any phase transition in the former will convey a singularity in the latter. However, a crucial requirement in order to accomplish this mapping is that the coupling in one spatial direction must be much stronger than the coupling(s) in the other direction(s). In particular, the imaginary time direction always corresponds to the direction of strong coupling. More information is given in appendix A.

In order to favour the step confinement without hindering the left–right meandering of primary steps typical of a DOF surface, a general method (alternative to switching on the interaction between the kinks) is, as we learned from experience on solid-on-solid (SOS) models (Prestipino *et al.* 1995), to extend the range of step repulsion in a suitable way. The simplest way to do so is by including a further term in equation (1), representing a repulsion between steps that are *second* neighbours. Precisely, we include in the VGL Hamiltonian a term $\sum_{m,y} g(u_{m+2}(y) - u_m(y))$, with

$$g(\Delta u) = \begin{cases} 0 & \text{for } \Delta u \geqslant -1, \\ U_3 & \text{for } \Delta u = -2, \\ +\infty & \text{for } \Delta u < -2. \end{cases} \tag{7}$$

It is evident from equation (7) that a supplementary cost of U_3 only appears for a horizontal separation of $3a$ between steps m and $m+2$. Although a similar interaction would generally exist in a real vicinal with a U_3 much smaller than U_1, it is worth considering here U_3 to be generic, in order to see whether the modified VGL model can sustain a DOF phase whatsoever. By extending the method of Villain *et al.* (1985), we show in appendix A how to map the extended VGL Hamiltonian on to the following 1D quantum problem:

$$H_{\mathrm{Q}} = -\frac{1}{2}\sum_{v=1}^{2N_x}(c_v^{\dagger}c_{v+1} + c_{v+1}^{\dagger}c_v) + J_z\sum_{v=1}^{2N_x} n_v n_{v+1} + J_3\sum_{v=1}^{2N_x} n_v n_{v+1} n_{v+2}, \tag{8}$$

where c_v and $c_v^{\dagger}$ (for $v = 1, \ldots, 2N_x$) are anticommuting spinless-fermion operators, $n_v = c_v^{\dagger}c_v$ is the number (charge) operator, $J_z = [\beta U_1 \exp(\beta W_1)]/2$, and $J_3 = [\beta U_3 \exp(\beta W_1)]/2$. In particular, both J_z and $J_3 = (U_3/U_1)J_z$ are increasing functions of $\beta = 1/(k_{\mathrm{B}}T)$. The free energy of the modified VGL model is the same as the ground-state energy E_0 of equation (8), on condition that $\beta U_1, \beta U_3 \ll 1 \ll \beta W_1$, and provided that the 1D lattice is half-occupied (see appendix A).

The ground state of equation (8) at half-filling cannot be easily calculated; thus an approximation scheme is in order, and the most natural by far, when different

ground-state structures compete together to give the lower energy, is the variational method. In this scheme, a number of trial (solvable) Hamiltonians is considered, each containing one or more adjustable parameters, and the ground-state average $\langle 0|H_Q|0\rangle$ is calculated for each. For given values of U_3/U_1 and J_z, the physical solution will be that providing the lower minimum of $\langle 0|H_Q|0\rangle$ in the parameter space. Obviously, in order to keep contact with the original statistical problem, only those trial Hamiltonians are to be used whose ground state is in a clear correspondence with a surface phase. Following Santoro *et al.* (1996), we choose a site-centred charge density wave (CDW) with a wavelength of two lattice spacings as the quantum-mechanical counterpart of an ordered flat surface, while we take a bond-centred CDW (of equal wavelength) as representing a DOF surface. This can be rationalized as follows. Consider first the perfectly ordered surface; with the same notations as in appendix A, we have $v_m(y) = 2m$ for all y, so that $-\frac{1}{2}$ and $\frac{1}{2}$ spins strictly alternate, and the same occurs for n_v between 0 and 1. Conversely, a spin state where the charge is peaked on one bond every two is the exact counterpart of a surface having an effective half-integer $v_m(y)$ equal, for all m and y, either to $2m + \frac{1}{2}$ or to $2m - \frac{1}{2}$, that is each step position is on average $\frac{1}{2}$ or $-\frac{1}{2}$, respectively, as expected in a DOF surface.

In appendix B, the two competing estimates of the ground-state energy of the Hamiltonian (8) are derived, namely $E_S(U)$ for a site-centred CDW and $E_B(U)$ for a bond-centred CDW, where U is an adjustable amplitude. Both variational estimates are functions of U_3/U_1 and J_z, while U is tuned to obtain the minimum possible energy. If the absolute minimum falls at $U = 0$, then the XY (tight-binding) solution takes over, corresponding to a stable rough phase.

For a fixed U_3/U_1, the temperature is varied acting on J_z. We first consider the standard VGL model ($U_3 = 0$). In this case, roughening occurs for $J_z \approx 0.4$ (instead of 1 as in equation (3)), and there is no PR, that is the DOF phase never acquires more stability than the ordered flat (OF) phase. Next, we set $U_3 = U_1$. Also in this case, however, we find that the DOF phase is never stable within our mean-field approach, while roughening is found to occur at $J_z \approx 0.11$, that is the roughening temperature has moved upwards with respect to $U_3 = 0$. By strengthening U_3 substantially, we expect that the DOF phase will eventually appear. In fact, for example, for $U_3 = 5U_1$, roughening has moved down to $J_z \approx 0.04$, while a PR transition now appears at $J_z \approx 0.5$, accompanied by a jump in U, which is hence first order.

In conclusion, we found that a sufficiently strong U_3 coupling is able to stabilize the DOF phase in a range of temperatures that becomes wider, the larger U_3 is compared with U_1. However, very large values of U_3/U_1 (larger than 1) are needed, at least within mean-field theory, to promote the DOF phase, and this makes the picture rather unrealistic. In view of this, we believe that the only mechanism of practical relevance for stabilizing the DOF phase in a vicinal is a strong repulsion between parallel kinks. It remains to be seen whether this is realized in a given model. In the following section, the specific case of a fcc metal (115) surface is considered, given that accurate STM measurements are available for Ag(115).

§4. What phases occur in the modified terrace–step–kink model?

Now, we report the results of a detailed Monte Carlo (MC) analysis of the MTSK model (equations (5) and (6)) designed to model a fcc metal (001) vicinal surface such as the Ag(115) surface. The main outcome of this study is the following: if the short-range repulsion between parallel kinks is strong enough, the vicinal exhibits three different phases: a low-temperature OF phase, an intermediate DOF

phase and a rough phase at high T. On the other hand, a weaker repulsion between the kinks is insufficient to stabilize the DOF phase, and the roughening behaviour will be the same as for the VGL model.

As a preliminary test, we check our MC program (see description below) against exact results. With this aim, we carry out transfer-matrix calculations for a strip of four steps. The strip is infinitely long in the y direction, while PBCs hold along x. For our purposes, it is convenient to rewrite the Hamiltonian as $N_x N_y(U_1 E_{U_1} + W_1 E_{W_1} + \cdots)$, where the remainder does not depend on U_1 and W_1; then, the following relation holds, involving the exact free energy per site:

$$\left(\frac{\partial \beta f}{\partial \beta U_1}\right)_{W_1/U_1,\beta U_2,\beta W_2,\beta W_3} = \langle E_{U_1}\rangle + \frac{W_1}{U_1}\langle E_{W_1}\rangle. \tag{9}$$

We set $\beta U_2 = \beta W_2 = \beta W_3 = +\infty$ and $W_1 = 10U_1$, and we vary βU_1 from 0 to 0.3. While the free-energy derivative on the left-hand side of equation (9) is evaluated numerically from the transfer-matrix data, the right-hand side is obtained from the simulation. The lattice is 4×400 in this case and 2.5×10^6 sweeps are generated at equilibrium, 1 sweep consisting of one average attempt per site to change the local u value by ± 1. By looking at figure 3 (b) it is clear that the quantities on the two sides of equation (9) are undoubtedly the same.

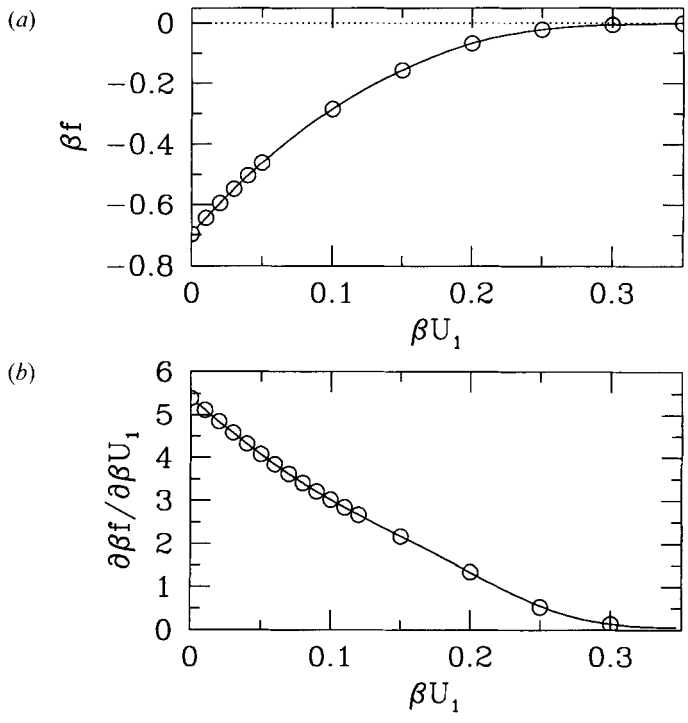

Figure 3. Check of our MC program for the MTSK model through a comparison with exact transfer-matrix results. We use $W_1 = 10U_1$ and $U_2 = W_2 = W_3 = +\infty$. ($a$) Exact free energy per site of a $4 \times \infty$ lattice strip: (——), spline interpolant which, by construction, has zero derivative at the boundaries. (b): MC results (○) for the right-hand side of equation (9), together with the numerical derivative of the above-mentioned interpolant (——).

Next, we prove the existence of a DOF phase in the MTSK phase diagram. The most favourable situation from the DOF is when U_2, W_2 and W_3 are all infinite. We take $W_1 = 20U_1$ and vary βU_1 from 0 to 0.18. We use standard Metropolis MC simulation and PBCs. The lattice consists of N_y positions for each of a number N_x of steps. A MC move consists of a local updating of u, which is changed by ± 1 at given m and y chosen at random; then, the move is accepted or rejected according to the usual Metropolis rule (the move is always rejected if any of the constraints embodied into the model is going to be violated). After due equilibration of the sample, as many as 1.5×10^6 sweeps are generated. Averages are updated every 10 MC sweeps. Besides other quantities, we calculate the mean square step lateral excursion $\delta u^2 = \langle [u_m(y) - \overline{u_m}]^2 \rangle$ (with $\overline{u_m} = \sum_y u_m(y)/N_y$), the parity order parameter $P = \langle (-1)^{u_m(y)} \rangle \approx \langle \mathcal{P} \rangle$, with $\mathcal{P} = |\sum_{m,y} (-1)^{u_m(y)}/(N_x N_y)|$, and the order-parameter susceptibility $\chi_P = N_x N_y (\langle \mathcal{P}^2 \rangle - \langle \mathcal{P} \rangle^2)$. We expect that strong antiparallel correlations between consecutive kinks in the same step will result, in the thermodynamic limit, into a vanishing P and a finite δu^2, which will characterize the DOF phase if present. In that case, if PR is critical, δu^2 is expected (Prestipino and Tosatti 1999) to increase logarithmically at T_{PR}.

To corroborate our conclusions, we spend some more time on the evaluation of the statistical uncertainties affecting the relevant averages. As usual, these are defined as rms deviations of statistical averages, once many independent estimates of these quantities (block averages) are made. For most quantities, grouping MC states in blocks of 10^5 sweeps suffices for all purposes. However, particular care must be taken for the susceptibility, whose values could be correlated over much longer segments of MC trajectory than 10^5 sweeps. Finally, errors are particularly severe close to second-order transition points, owing to unlimited growth of decorrelation times.

In figure 4, simulation data are plotted for three values of N_x, namely 8, 16 and 24 (we take $N_y = 20N_x$). Although such step numbers are not very large, the clear-cut maximum of δu^2 is the most likely signal of a PR phase transition occurring at $\beta U_1 \approx 0.08$ (a logarithmic increase in this maximum with increasing system size is roughly consistent with our data). Moreover, beyond that temperature, δu^2 remains finite in the thermodynamic limit, even at the infinite temperature, meaning that the rough phase is totally absent in this case, so that the high-temperature phase of the model is DOF (statistical errors are so small that the above conclusions are safe). As a result, the vicinal surface would be rough only at the isolated PR point, and flat both below and above. Therefore, infinite parallel-kink repulsion effectively acts to confine the steps around $u = 0$ at any temperature without, however, hindering a strictly left–right zigzagging of steps at high temperature. This meandering contributes a large entropy to the steps which lowers the surface free energy, thus counterbalancing the energy cost for kinks. As to the order of the PR transition, we find that χ_P diverges at T_{PR} while the specific heat remains finite (see figure 4, inset). Hence, PR is second order with a negative specific-heat exponent.

In figure 5, a small part of the vicinal at $U_1 = 0$ is shown. This picture reveals what is the general structure of the DOF phase; kinks are very numerous along the steps but the correlation between two consecutive kinks is strictly antiparallel, so that the overall surface is flat; its slope on the x–y plane the same as for the perfect vicinal surface. Indeed, the DOF state in figure 5 is nearly ideal; each of the steps strictly meanders between two positions with equal probability; hence $\delta u^2 \approx 0.25$. In

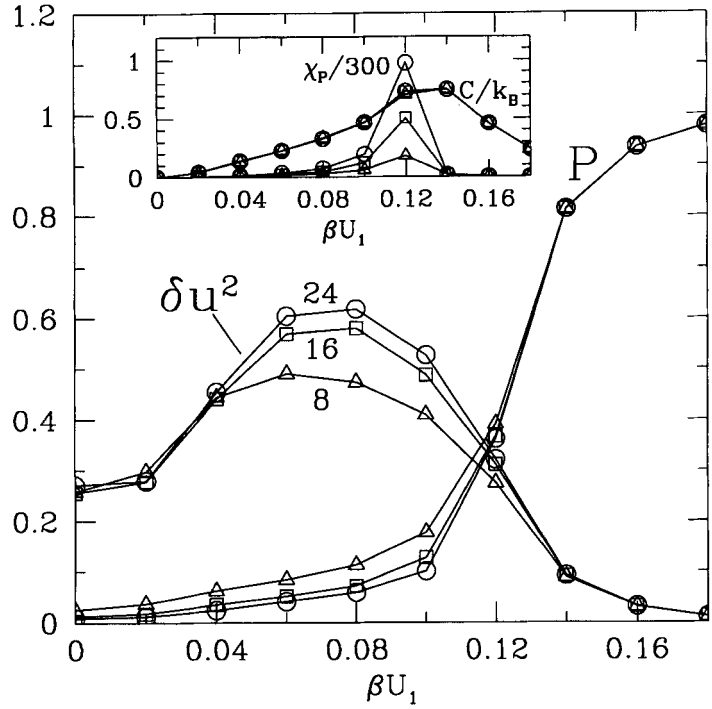

Figure 4. MTSK model: MC data for three different step numbers, $N_x = 8$ (△), $N_x = 16$ (□) and $N_x = 24$ (○), with $N_y = 20N_x$ in each case. Here, the parameters are chosen to be $W_1 = 20U_1$ and $U_2 = W_2 = W_3 = +\infty$. Results are shown for P and δu^2. Error bars are smaller than the symbol sizes. In the inset, the results for χ_P and the specific heat are shown. A rather sharp PR transition occurs at $\beta U_1 \approx 0.08$, and no rough phase is observed in this case. Although general arguments suggest a logarithmic growth of δu^2 at $T = T_{PR}$ as a function of the surface size, our samples are too small (and too few) to extract this behaviour from the data.

practice, a real DOF surface will be generally characterized by a δu^2 value substantially larger than 0.25, owing to defects superimposed on the ideal DOF pattern.

The tendency of kinks towards antiparallel order can be measured by the relative amount of kink–antikink pairs with respect to kink–kink neighbour pairs. Both in the DOF and in the ordered phase, there is a comparatively lower number of consecutive parallel kinks than near T_{PR}, implying that the absolute density of kink–kink neighbour pairs has a maximum close to T_{PR} (figure 6).

Further independent evidence of the DOF phase comes from the measurement of the free-energy cost of a kink. This is defined as $\eta_1 = N_y\beta(f_1 - f_0)$, where f_0 is the free energy per site when full PBCs are applied and f_1 is the same quantity after insertion of one further kink in each step. In order to perform this, the use of proper 'periodic-kink boundary conditions' along y is mandatory. The standard method for η_1, which makes use of the transfer matrix (Den Nijs and Rommelse 1989, Prestipino and Tosatti 1997), does not work in this case; calling x the direction of transfer and given a configuration for the mth step, the number of possible states for step $m + 1$ is not bounded, since there is no upper limit for the distance between two adjacent steps in the MTSK model, that is there are not enough constraints to keep the 'coordination number' of a step state finite when the number of steps goes to infinity.

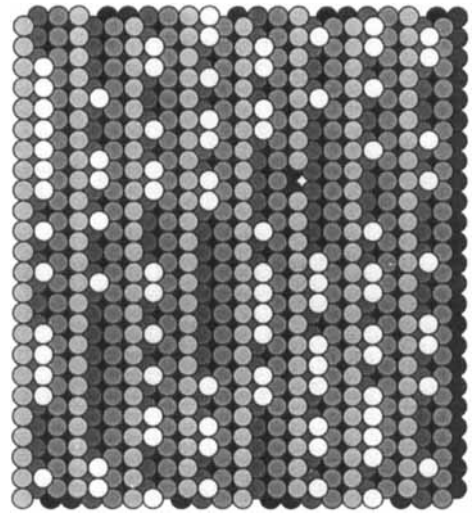

Figure 5. A snapshot from the same MC simulation as in figure 4. The view is from [115]. Here, $N_x = 16$ and $\beta U_1 = 0$ (only a small part of the lattice with eight steps is shown). Left and right kinks strictly alternate along the steps, leading to an almost perfect realization of a DOF surface (i.e. $\delta u^2 \approx 0.25$).

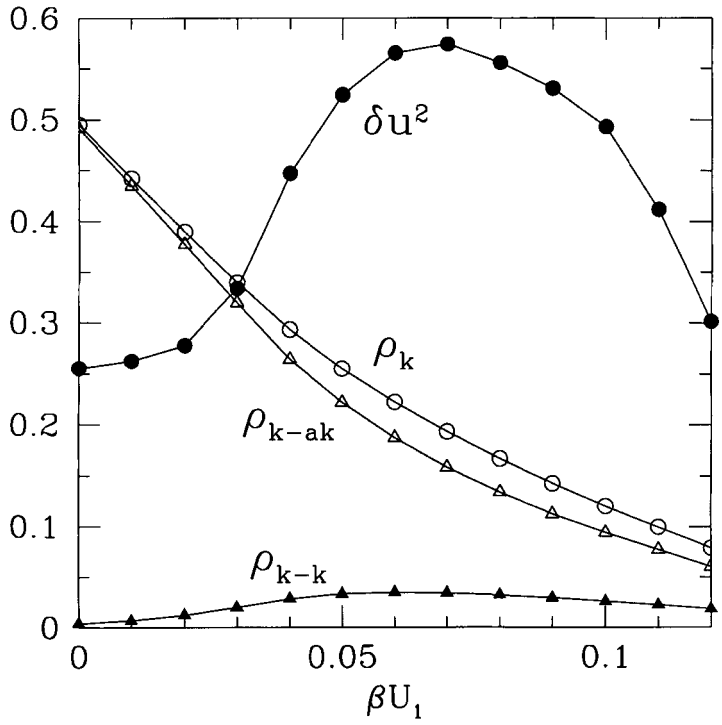

Figure 6. MTSK model: MC data for $N_x = 16$ and $N_y = 320$, with $W_1 = 20U_1$ and $U_2 = W_2 = W_3 = +\infty$. Results are shown for the kink density ρ_k, the density $\rho_{k\,ak}$ of consecutive antiparallel kinks, and the density $\rho_{k-k} = \rho_k - \rho_{k-ak}$ of consecutive parallel kinks (error bars are smaller than the symbol sizes). The normalization is such that, for example $\rho_k = \frac{1}{2}$ means a kink every two step positions while, for example $\rho_{k-ak} = \rho_k$ indicates 100% of kink–antikink neighbour pairs.

This notwithstanding, at least the thermal derivative of η_1 can be obtained in a MC experiment by inserting a right kink in each step and recording the change in E_{U_1} and E_{W_1}. In fact, using equation (9), one has

$$\left(\frac{\partial \eta_I}{\partial \beta U_I}\right)_{W_1/U_1,\beta U_2,\beta W_2,\beta W_3} = N_y\left((\langle E_{U_1}\rangle_1 - \langle E_{U_1}\rangle_0) + \frac{W_1}{U_1}(\langle E_{W_1}\rangle_1 - \langle E_{W_1}\rangle_0)\right). \quad (10)$$

By its very definition, η_1 is non-zero in any flat phase (where steps are straight on average), while it is expected to vanish as N_y^{-1} at a second-order PR and in the whole rough phase (owing to N_y^{-2} scaling of free energies at criticality) (Den Nijs and Rommelse 1989). In a finite system, η_1 will be a minimum at a temperature T^* close to T_{PR}, hence the thermal derivative of η_1 will be negative for $T < T^*$ and positive for $T > T^*$. Indeed, considering that

$$\frac{\partial \eta_I}{\partial (k_B T/U_I)} = -\beta^2 \frac{\partial \eta_I}{\partial \beta U_I}, \quad (11)$$

this is what we observe (figure 7(*a*)). On the contrary, no such feature is present when PR is not seen, as for instance in the VGL model (figure 7(*b*)). This indicates

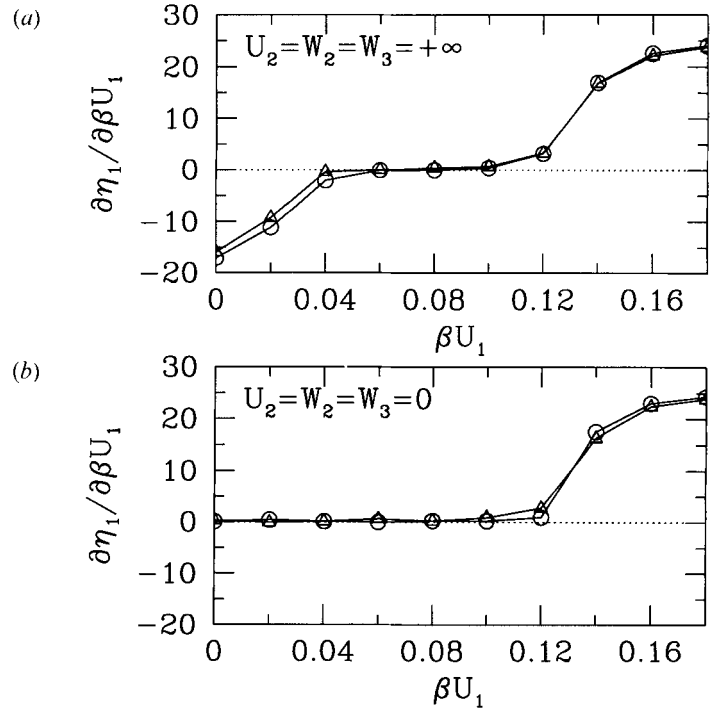

Figure 7. Derivative of the kink free energy with respect to inverse temperature: (*a*) MTSK model, with $W_1 = 20U_1$ and $U_2 = W_2 = W_3 = +\infty$; (*b*) VGL-like model ($W_1 = 20U_1$ and $U_2 = W_2 = W_3 = 0$). Results are shown for $N_x = 8$ (△) and $N_x = 16$ (○), 1.5×10^6 sweeps are produced at equilibrium. Error bars are at most comparable with the symbol sizes. Negative values of the free-energy derivative for low βU_1 are the fingerprint of the DOF phase which sets in at $\beta U_1 \approx 0.08$ in (*a*). A zero value for the same quantity above a certain temperature is clear evidence for the rough phase in (*b*).

that we need U_2 and W_2 (or, at least, one of them) to be very large in order to observe both PR and roughening.

To prove this, we perform an extensive MC simulation of the MTSK model for $W_1 = 20U_1$, $U_2 = W_2 = 2000U_1$ and $W_3 = 0$. In figure 8, we plot the average square step displacement δu^2 and the order parameter P (error bars are of the same size as symbols or smaller). From their behaviour, we conclude that all three phases are present, the DOF phase being stable in the interval between $\beta U_1 \approx 0.0007$ and $\beta U_1 \approx 0.05$ (note that $T_{PR}/T_R \approx 0.014$). PR is probably second order here. We also monitor the u values during the run and find that, inside the DOF region, the current mean step position $\bar{u}$ takes the same half-integer value for all steps, with occasional jumps during the run from a half-integer number to the next (left or right), which are more frequent for smaller surface size. This behaviour closely resembles that originally observed in the DOF phase of the face-centred SOS model (Prestipino *et al.* 1995). Further note that a positive W_3 is unnecessary for the very existence of PR. The only effect of including W_3 is to shift the PR temperature downward, so as to increase the extent of the DOF region (see also figure 4).

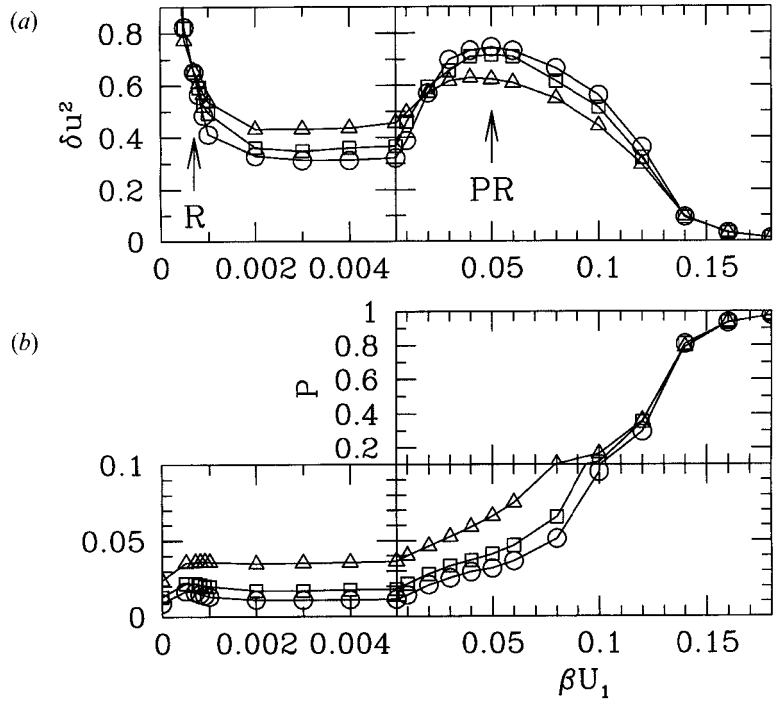

Figure 8. MC results for the MTSK model of equations (5) and (6), with $W_1 = 20U_1$, $U_2 = W_2 = 2000U_1$ and $W_3 = 0$. (*a*) The average square kink displacement δu^2 and (*b*) the order parameter P are shown as functions of the inverse temperature βU_1 for lattices that are very elongated in the y direction, $N_y = 20N_x$ for $N_x = 8$ (△), $N_x = 16$ (□) and $N_x = 24$ (○). After equilibration, from 3×10^6 to 5×10^6 sweeps are generated. Error bars are not shown since they are smaller than the symbol sizes. The surface is rough at high temperatures ($\beta U_1 < 0.0007$). The δu^2 maximum at $\beta U_1 \approx 0.05$ indicates PR at this temperature in the infinite-size limit. Note that $W_3 > 0$ is not really essential for PR. Removal of W_3 has only the effect of shifting T_{PR} upwards, thus reducing the interval of stability of the DOF phase (see figure 4).

It is interesting to explore the evolution in temperature of the kink free energy η_1 in this case. In figure 9, its derivative is plotted:

$$\left(\frac{\partial \eta_l}{\partial \beta U_l}\right)_{W_1/U_1, U_2/U_1, W_2/U_1, \beta W_3} = N_y\left((\langle E_{U_1}\rangle_1 - \langle E_{U_1}\rangle_0) + \frac{W_1}{U_1}(\langle E_{W_1}\rangle_1 - \langle E_{W_1}\rangle_0) + \frac{U_2}{U_1}(\langle E_{U_2}\rangle_1 - \langle E_{U_2}\rangle_0) + \frac{W_2}{U_1}(\langle E_{W_2}\rangle_1 - \langle E_{W_2}\rangle_0)\right), \tag{12}$$

whose thermal evolution should be compared with that of figure 7(*a*). Using equation (11), it is not difficult to deduce from figure 9 the following description of $\eta_1(T)$ in the thermodynamic limit: η_1 is positive at low temperature, vanishing first at $T_{PR}(\beta U_1 \approx 0.05)$. On heating, it recovers a positive value in the DOF phase until it vanishes again and for ever upon reaching the roughening temperature T_R ($\beta U_1 \approx 0.0007$). As a result, proliferation of kinks and concurrent delocalization of steps first occur at T_{PR} but, owing to a non-zero η_1 value between T_{PR} and T_R, kinks maintain a strong antiparallel correlation in the DOF phase, causing steps to

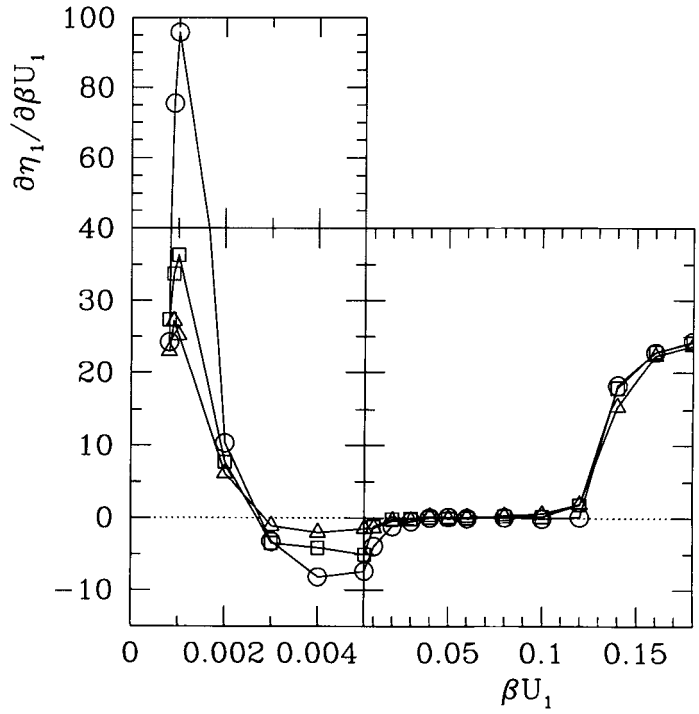

Figure 9. Derivative of the kink free energy with respect to the inverse temperature for $W_1 = 20U_1$, $U_2 = W_2 = 2000U_1$ and $W_3 = 0$. Data are plotted for $N_x = 8$ (△), $N_x = 16$ (□) and $N_x = 24$ (○). From 3×10^6 to 5×10^6 sweeps are produced at equilibrium. Near $\beta U_1 = 0.005$, the largest errors are comparable with the symbol sizes. From this picture, the following infinite-size behaviour of η_1 is deduced: η_1 is positive in both the flat phases, while it is zero at PR ($\beta U_1 \approx 0.05$) and in the whole rough phase ($\beta U_1 < 0.0007$).

remain straight on average. One must wait until T_R for the steps to become delocalized again, this time permanently.

Another interesting subject is that of correlations between the kinks. We study in detail the character of such correlations for $N_x = 24$, which is our largest system size. In particular, the relative orientation of consecutive kinks has been investigated, finding a clear bias towards antiparallel correlation in the whole interval of temperatures where the DOF phase is stable. In figures 10 and 11, we show the profile of the correlation function

$$G(m, y) = \langle [u_m(y) - u_0(0)]^2 \rangle, \tag{13}$$

as a function of both m (for $y = 0$) and y (for $m = 0$), for a number of βU_1 values in the relevant temperature range (note that $G(0, 1) = \langle E_{W_1} \rangle$ is the kink density). Superimposed on it is a logarithmic least-squares fit drawn from the work of Selke and Szpilka (1986) and also used by Hoogeman *et al.* (1999) and Hoogeman and Frenken (2000):

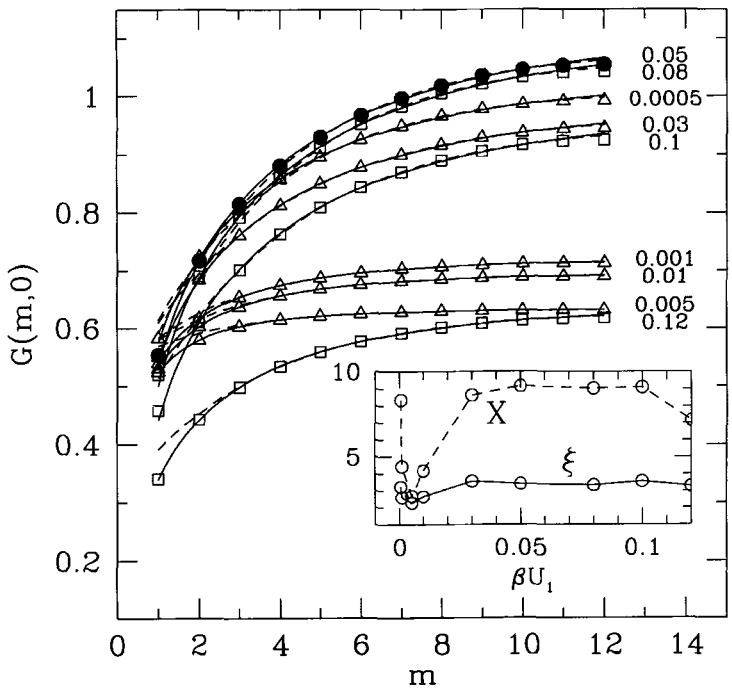

Figure 10. Kink-kink correlations $G(m, 0)$ along the x direction for $N_x = 24$, with the same MTSK parameters as in figure 9. G values are updated every 5000 sweeps: (——) best (i.e. least-squares) fits obtained from equation (14) after discarding the first ($m = 1$) and the last ($m = 12$) point; (- - - -) best fits obtained from equation (15) in the range of values between $m = 5$ and $m = 10$. The numbers on the right are βU_1 values, and different symbols are used for $\beta U_1 < 0.05$ (△), $\beta U_1 = 0.05$ (●) and $\beta U_1 > 0.05$ (□). Error bars are much smaller than the symbol sizes. In the inset, the corresponding estimates of X and ξ_x are provided, suggesting roughening at $\beta U_1 \approx 0.0005$ and PR somewhere between, say, $\beta U_1 = 0.05$ and 0.1. In the thermodynamic limit, ξ_x is expected to grow exponentially as a function of $T_R - T$ when T goes to T_R from below, while a power-law divergence is expected near T_{PR}.

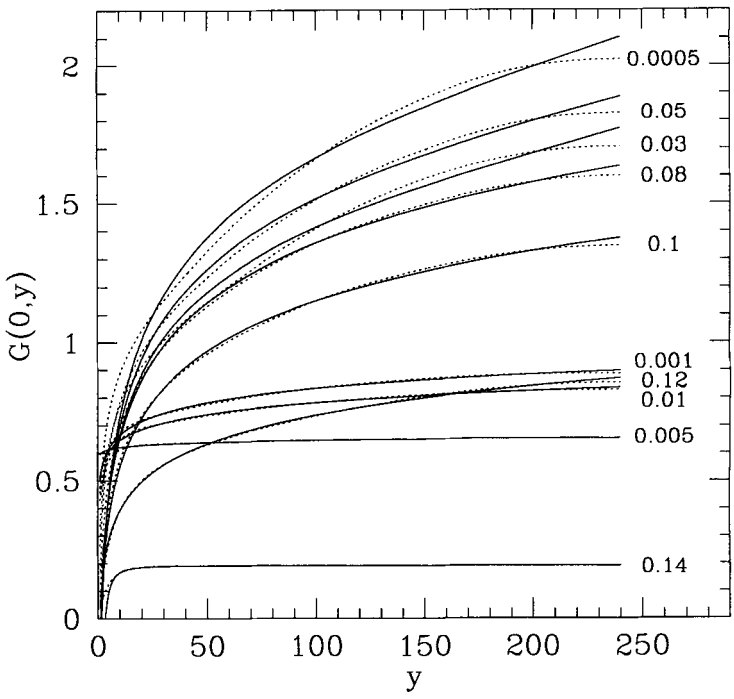

Figure 11. Kink–kink correlations (.....) along the y direction for $N_x = 24$, with the same MTSK parameters as in figure 9. (——) least-square fits obtained with the use of equation (14) in the interval between $y = 11$ and $y = 230$. The numbers on the right are βU_1 values. Statistical errors are not relevant. It is evident that the G data are not well fitted over the entire y range to equation (14); hence our best X and K (not shown) are poorly significant. Anyway, it can be still deduced from this picture that the steps are spatially localized in the DOF region, between $\beta U_1 = 0.0007$ and 0.05.

$$G(m,0) \simeq -\frac{K(T)}{2} \ln [m^{-2} + X(T)^{-2}] + C(T). \tag{14}$$

In fact, in order to extract the correlation lengths along x and y, a more natural choice would have been to use, for the large-distance profile of $G(m,y)$, the behaviour typical of a Gaussian model (Prestipino and Tosatti 1999), namely

$$G(m,0) \sim K\left(\ln \xi_x - \left(\frac{\pi\xi_x}{2m}\right)^{1/2} \exp\left(-\frac{m}{\xi_x}\right)\right), \tag{15}$$

for $m \gg 0$, and

$$G(0,y) \sim K\left(\ln \xi_y - \left(\frac{\pi\xi_y}{2y}\right)^{1/2} \exp\left(-\frac{y}{\xi_y}\right)\right), \tag{16}$$

for $y \gg 0$. This behaviour has a far more solid foundation than equation (14), whose leading $\mathcal{O}(m^{-2})$ correction to the asymptotic $K \ln X$ form has no theoretical justification. However, the fit (14) proves to be more effective, in the whole range of x distances, than the exponential fit (15). Moreover, information about the location of phase transitions is equally accurate from the fit (14). In fact, although X is not the correlation length, X and ξ behave similarly at any temperature, since they are

both finite or both infinite. In particular, the transition points are both characterized by a very large X value, as demonstrated in figure 10, inset. Obviously, the behaviours of X and ξ reported in figure 10 is of mostly qualitative significance; no finite-size study of these quantities has been attempted; thus no clear proof can be obtained from figure 10 of the divergence of X and ξ at PR and in the whole rough phase.

Equally not reliable, owing to the small size of the system along x and to the intrinsic inaccuracy of the formula, is the value of K that is extracted from the logarithmic fit, at least in the PR region. Although the universal $2/\pi^2$ value of K at roughening (see appendix C) is consistent with the value (0.22) that we find at $\beta U_1 = 0.0005$, K is expected (Prestipino and Tosatti 1999) to take at PR a non-universal value smaller than $2/\pi^2$, while in fact we find it to be larger ($K \approx 0.27$).

In figure 11, we plot $G(0, y)$ for the same temperature values as in figure 10. This time, neither the exponential fit nor the logarithmic fit works well in the whole range of y values. Incidentally, the optimal X or ξ are one order of magnitude larger than the same quantities for $G(m, 0)$; this is due to the anisotropy of the problem, that is to the fact that $W_1 \gg U_1$.

To conclude, the DOF phase is stable in the MTSK model at least when both U_2 and W_2 take a very large value. Moreover, PR appears to be critical even when $T_{PR} < T_R/4$, contrary to the expectation founded on a variational theory of PR (Prestipino and Tosatti 1999). At present, the question as to whether a set of MTSK parameters exists which leads to a first-order PR remains unanswered. In the next section, we shall move to a possible MTSK modelling of Ag(115), seeking for clues of a DOF behaviour in some temperature interval around 460 K.

§ 5. The case of Ag(115)

In a recent STM study (Hoogeman *et al.* 1996), the kink formation energy and the step repulsion of Ag(115) were measured at room temperature, thus providing values for W_1 and U_1. These couplings have been independently estimated; while W_1 is essentially calculated from the density of kinks along a $[\bar{1}10]$ secondary step, U_1 is evaluated through the fluctuations in the relative position of kinks along secondary steps running close to the $[55\bar{2}]$ direction. In particular, a value is obtained for U_1 of 19 K (half of the value reported by Hoogeman *et al.* (1996); the step repulsion per atom in our model is actually $2U_1$).

The kink energy could in principle be determined through the measurement of the density of kinks along primary steps. In fact, a kink is always accompanied by a shortening of distance between two neighbouring steps, that is by a supplementary cost due to step repulsion of $2U_1$ per atomic position. If U_1 is unknown, the only possibility of determining W_1 is to consider step configurations where a broadened terrace of width $3.5a$ appears in the vicinal owing to a local surface misorientation, a likely event in a real surface. This induces in the surface a $[\bar{1}10]$ secondary step, whose cost of meandering does not involve U_1. In fact, the kink density depends only on W_1 in this case and is estimated to be (Hoogeman *et al.* 1996)

$$p = [1 + \tfrac{1}{2}\exp(\beta W_1)]^{-1}. \tag{17}$$

From the observed density of kinks on $[\bar{1}10]$ secondary steps, $p = 0.019$, it thus follows that $W_1 = 1323$ K. Equation (17) should be contrasted with the expression $p = [1 + \exp(\beta W_1)]^{-1}$ which refers to a $[\bar{1}10]$ secondary step obliged to run parallel to the y direction (see appendix D).

Hoogeman *et al.* (1996) reported the statistics of kinks only for step configurations where no two consecutive parallel kinks are present. Thus, no clue can be obtained from the STM study as to the strength of the short-range kink–kink interaction in Ag(115). Since a value of 260 K was reported for the repulsion between kinks in neighbouring steps, we tentatively assume that as the value of U_2. The problem remains as to the values that must be attributed to W_2 and W_3. Since we do not know how to estimate W_2 and W_3 for Ag, we tentatively assume them to be infinite (i.e. very large). The rationale behind this choice is that, if no PR occurs with $W_2 = W_3 = +\infty$, which is the most favourable situation for the occurrence of PR, then it would be impossible to support the view of a DOF phase in Ag(115), within the strict MTSK model.

With the above parameters, we carry out a MC simulation of the MTSK model, with $N_x = 8, 16, 24, 32$ and $N_y = 30N_x$ in all cases, since the aspect ratio of a correlated region, that is the ratio of the correlation lengths in the y and x direction, should be close to $W_1/(2U_1)$, at least far from criticality. From 4×10^6 to 8×10^6 sweeps are produced at equilibrium. Simulation data are reported in figure 12. First, we note that, notwithstanding 8×10^6 sweeps are a huge number of MC moves, the relevant averages are still affected by an appreciable error, especially so for the larger sizes. However, there is indication that the order parameter goes to zero at about 410 K, where its susceptibility diverges, suggesting a second-order phase transition which can be either roughening or PR. In principle, the profile of δu^2 should allow us to discriminate between the two possibilities. However, the errors on data points are so large that no sharp conclusion is allowed on the existence of PR in this case (error bars on the δu^2 data are of the same size as symbols in figure 12).

Some clue about the nature of the phase transition at 410 K can nonetheless be obtained from the following considerations. When $W_1 = 20U_1$ and all the other MTSK parameters are infinite, PR falls at $T_{PR} \approx U_1/0.08 = 240$ K (§ 4). Similarly, we have verified that, when the ratio of W_1 and U_1 is 60 (i.e. the same as for Ag(115)) and $U_2 = W_2 = W_3 = +\infty$, the rough phase is still absent but PR has moved to $T_{PR} \approx U_1/0.03 = 630$ K. Now, a large but finite U_2 (as in the case of the MTSK modelling of Ag(115)) can hardly affect PR in such a way that T_{PR} becomes substantially lower than 630 K; rather, it will certainly stabilize the rough phase beyond a certain temperature. In particular, if roughening were to occur too early, that is well before 630 K, PR would be washed out and the DOF phase will not appear. This suggests that the phase transition found at 410 K is just ordinary roughening.

A further piece of evidence comes from the kink–kink correlations which have been characterized experimentally (Hoogeman *et al.* 1999, Hoogeman and Frenken 2000). We use equation (14) to fit the data, which proves to be good over the entire range of distances, at least for correlations in the direction perpendicular to the steps. According to the Kosterlitz–Thouless picture for roughening, $K(T)$ would be an increasing function of T, attaining the value of $2/\pi^2$ at roughening; moreover, the quantity $(K - 2/\pi^2)^2$ would be proportional to $T - T_R$, for $T \gtrsim T_R$.

In figure 13, we plot $G(m, 0)$ for $N_x = 32$ as a function of m (up to $m = N_x/2 = 16$) for various temperatures. The best-fit parameters are in turn shown in figure 14 for both $N_x = 24$ and 32. These results are consistent with the view that only a single roughening transition exists, somewhere between 410 and 420 K, within the MTSK model and with this choice of parameters. Moreover, X apparently saturates beyond 410 K (seemingly, at the largest value as possible for the

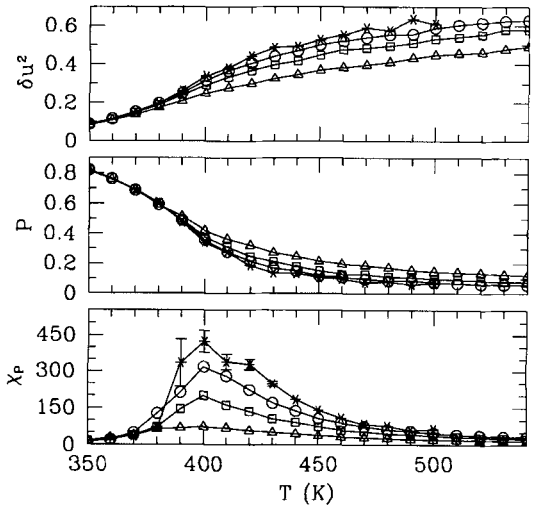

Figure 12. MC simulation data for the MTSK model with $U_1 = 19\,\mathrm{K}$, $W_1 = 1323\,\mathrm{K}$, $U_2 = 260\,\mathrm{K}$ and $W_2 = W_3 = +\infty$. Data are plotted for $N_x = 8$ (△), $N_x = 16$ (□), $N_x = 24$ (○) and 32 (*) with $N_y = 30N_x$ in each case. Averages are calculated over 4×10^6 sweeps for $N_x = 8$ and 16 and over 8×10^6 sweeps for $N_x = 24$ and 32. Error bars on the susceptibility data for $N_x = 32$ are indicated (decorrelation times are of the order of 1×10^6 sweeps near $T = 400\,\mathrm{K}$; this is estimated through a comparison of averages calculated by grouping MC states in blocks of increasing length; the value of χ_P roughly saturates for block dimension larger than 1×10^6 sweeps). The susceptibility peak could either indicate PR, or simply roughening (see text).

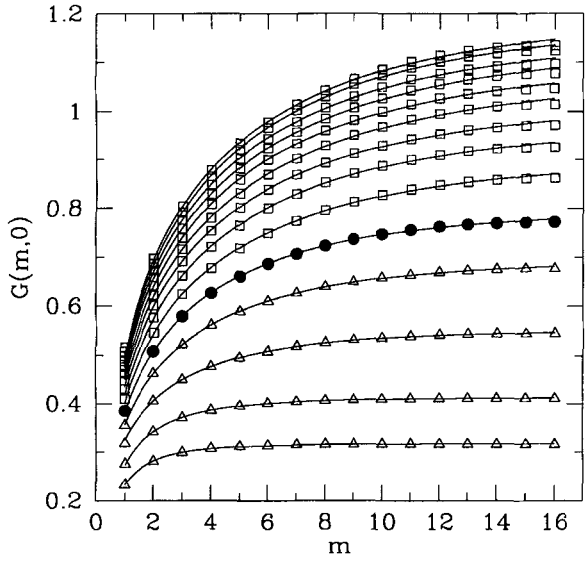

Figure 13. MTSK model, with the same parameters as in figure 12. (——), least-squares fits according to equation (14) in the interval between $m = 2$ and $m = 15$. Here, $N_x = 32$ and $N_y = 960$. The picture shows the kink–kink correlation function along x for $T = 370\,\mathrm{K}, 380\,\mathrm{K}, \ldots, 500\,\mathrm{K}$. Different symbols are used for $T < 410\,\mathrm{K}$ (△), $T = 410\,\mathrm{K}$ (●) and $T > 410\,\mathrm{K}$ (□). Error bars are much smaller than the symbol sizes.

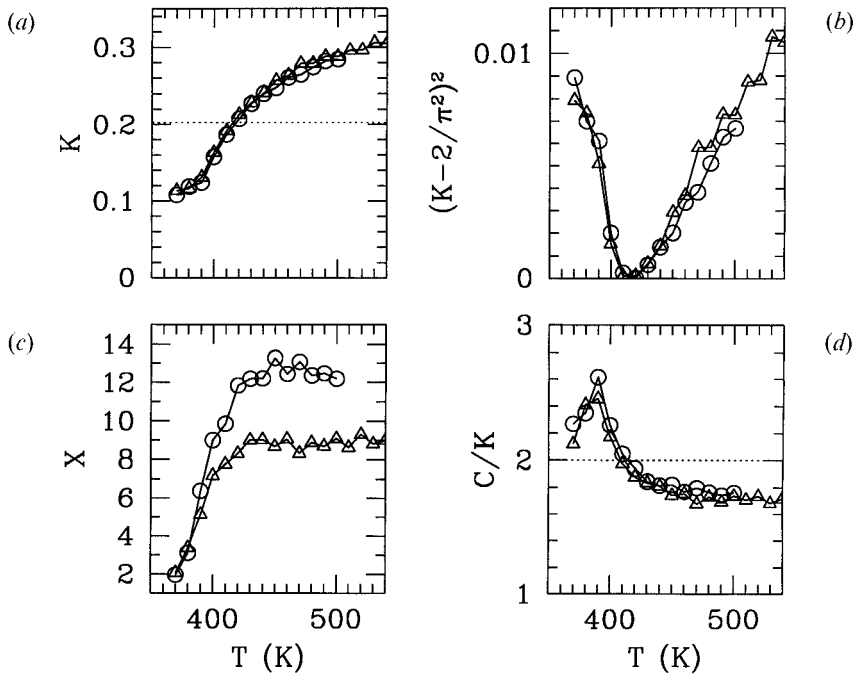

Figure 14. MTSK model, with the same parameters as in figure 12. Best fit-parameters, based on equation (14), to the kink–kink data in figure 13, are plotted as functions of temperature. Data are plotted for $N_x = 24$ (△) and $N_x = 32$ (○). (*a*) In particular, K attains the universal $2/\pi^2$ value (.....) typical of roughening at $T = 410$ K. (*b*)–(*d*) Beyond this temperature, (*b*) $(K - 2/\pi^2)^2$ is approximately linear in T, (*d*) C/K is close to 2 and (*c*) X levels off at a large constant value. This behaviour of parameters is consistent with conventional roughening at 410 K.

given N_x). Beyond this temperature, the ratio of C to K is not far from 2, which is what one expects in the rough phase (Selke and Szpilka 1986).

In conclusion, with MTSK parameters chosen to model roughly Ag(115), we do not find a clear PR with a DOF phase below roughening. Either the DOF window is so narrow that much larger sizes and longer runs are needed, or else only roughening is present. In the latter case, which at the moment appears to be the more conservative conclusion, we obtain that parameters extracted from current STM data for Ag(115) (data which suggest a DOF phase between 440 and 490 K) do not lead in fact to PR and a DOF phase within the MTSK model. One possible defect of this model is its failure to include long-range interactions. In fact, effective kink–kink interactions are of a long-range nature and this could possibly turn the roughening behaviour of Ag(115) from conventional to two-stage, that is with PR.

§6. Conclusions

In a vicinal surface, there is a general tendency to develop a DOF phase, favoured by repulsive elastic interactions between steps and even more between parallel kinks. Alternatively, a DOF phase can be promoted by an extended repulsion between the steps, similar in spirit to SOS models of low-index facets. Although a DOF phase could in principle be stabilized by this mechanism too (§ 3), we believe

this is a far less realistic route to PR than kink–kink repulsion. We have built a MTSK model which allows for a *short-range* repulsion between parallel kinks in the same step and also between parallel kinks in neighbouring steps. Using mainly MC simulation, we have shown that a DOF phase indeed occurs in the MTSK model if kinks repel each other sufficiently strongly, even if only at short range. This is already a fine result, complementary to that obtained by Den Nijs and Rommelse (1989) for low-index surfaces.

In trying to find an experimental realization of vicinal PR, we have then reconsidered recent STM results for Ag(115) that might be interpreted as providing the evidence of a DOF phase in the interval 440–490 K. In order to test this conjecture, we have used parameters extracted from experimental data (Hoogeman *et al.* 1996). However, with this choice of parameters, our results with the MTSK model do not show any clear DOF phase.

We suspect that long-range parallel-kink repulsion could be an important missing ingredient. Since the inclusion of long-range kink–kink interactions into the MTSK model appears at first sight to be problematic, we cannot, at the moment, do better than suggest new experiments on Ag(115). Probably, a scattering experiment in antiphase or else a refinement of the STM experiment of Hoogeman *et al.* with a more thorough study of kink–kink correlations might decide whether the two-stage PR–roughening scenario here proposed for the thermal disordering of Ag(115) is realistic or not.

ACKNOWLEDGEMENTS

We are grateful to Michele Fabrizio, to Joost Frenken and to Eduardo Jagla for helpful discussions, and to M. S. Hoogeman for making his PhD thesis data available to us. We acknowledge support by Istituto Nazionale per la Fisica della Materia through a fellowship for S.P., and by Ministero dell'Università e della Ricerca Scientifica e Tecnologica COFIN99.

APPENDIX A

MAPPING OF THE MODIFIED VILLIAN–GREMPEL–LAPUJOULADE MODEL ONTO A QUANTUM SPIN CHAIN

We outline here the derivation of equation (8), by extending the method developed in Villain *et al.* (1985). However, we first recall how to map the thermodynamics of a classical D-dimensional statistical problem on the ground-state landscape of a $(D-1)$-dimensional quantum Hamiltonian (Fradkin and Susskind 1978; Kogut 1979). Although not all Hamiltonians are naturally suited to be mapped on to a quantum problem, nevertheless, when this is possible, a far deeper insight is obtained about the original statistical model, including a sketch of its overall phase diagram.

The transfer matrix (path integral) method lies at the heart of this mapping. Consider a general classical lattice Hamiltonian H and let y be a selected spatial direction. Then, the reduced Hamiltonian can be written as $\beta H = \sum_{y=1}^{N_y} L(S_y, S_{y+1})$, where, depending on D, y denotes a single site ($D = 1$), or an entire row of sites ($D = 2$), etc., and S_y is the generic system state on the $(D-1)$-dimensional manifold

orthogonal to y. We call N_s the total number of states on this manifold. PBCs are always implied.

Let $T_{a,b} = \exp[-L(a,b)]$ be the transfer matrix (the partition function Z of the model is the trace of T^{N_y}). Then, a useful connection with a quantum problem follows if we are able to determine a quantum system endowed with an N_s-dimensional Hilbert space, a mapping $a \to |a\rangle$ and a Hamiltonian H_Q such that either $T_{a,b} = \langle b| \exp(-a_y H_Q)|a\rangle$, with an arbitrary a_y; or, what is more easy to fulfil, $T_{a,b} = \langle b|(1 - a_y H_Q)|a\rangle$, but with a_y so small that the substitution $1 - a_y H_Q \approx \exp(-a_y H_Q)$ is authorized (i.e. the matrix elements between any two states of a basis should be almost the same for the two operators). In this event, it readily follows that $Z \approx \mathrm{Tr}[\exp(-\tau H_Q)]$, with $\tau = N_y a_y$ (the trace being viewed as either the partition function of the quantum system or its propagator in imaginary time $t = -i\hbar\tau$).

So far, N_y is general. A more interesting connection emerges in the thermodynamic limit $N_y \to \infty$, where a nice relation shows up between the free energy f of the classical model and the (non-degenerate) ground-state energy E_0 of the quantum model. In fact, $\tau \to \infty$ as well (even if small, a_y is a constant!), and

$$\mathrm{Tr} \exp(-\tau H_Q) = \exp(-\tau E_0)(1 + \mathcal{O}\{\exp[-\tau(E_1 - E_0)]\}), \tag{A 1}$$

in such a way that

$$\beta f = -\lim_{N_y \to \infty} \left(\frac{\ln Z}{N_y} \right) = -\lim_{\tau \to \infty} \left(\frac{a_y}{\tau} \ln \{\mathrm{Tr}[\exp(-\tau H_Q)]\} \right) = a_y E_0, \tag{A 2}$$

which links any phase transition in the classical model to a singularity in the ground-state energy E_0 of the quantum model. Similarly, the inverse correlation length of the original model can be shown to be simply proportional to the energy gap $E_1 - E_0$.

Having described the general method, we now apply it to the VGL model with an extended step–step repulsion (see equation (7)). We first repeat the rather concise derivation by Villain *et al.* (1985) in order to set the stage for its further generalization. We call l the terrace width and $x_m(y) = ml + u_m(y)$ the absolute position of the mth step ($m = 1, \ldots, N_x$) at row y and assume, for later convenience, a hard wall at the left lattice boundary $x = l - 1$ and another at the right boundary $x = N_x l$ (in the thermodynamic limit, any boundary effect will be negligible). We also define a new integer variable $v_m(y)$ as $v_m(y) = u_m(y) + 2m$, so that the constraint $u_{m+1}(y) - u_m(y) \geqslant -1$ becomes $v_{m+1}(y) \geqslant v_m(y) + 1$, while $v_1(y) \geqslant 1$ and $v_{N_x}(y) \leqslant 2N_x$. As a result,

$$1 \leqslant v_1(y) < v_2(y) < \cdots < v_{N_x}(y) \leqslant 2N_x. \tag{A 3}$$

For any $1 \leqslant v \leqslant 2N_x$, a spin S_v is defined as $S_v = \frac{1}{2}$ if $v_m(y) = v$ for some value of m, while $S_v = -\frac{1}{2}$ otherwise. In particular, we note that

$$\sum_{v=1}^{2N_x} S_v = 0. \tag{A 4}$$

Hence, a chain of $2N_x$ spins (with as many $\frac{1}{2}$ as $-\frac{1}{2}$) is associated with a row $\{u_m(y), m = 1, \ldots, N_x\}$ of step positions. We quantize these spins by associating hard-core boson, spin-$\frac{1}{2}$ operators σ_v with them. That is to say, σ_v^+ and σ_w^- are taken to commute on different sites ($v \neq w$), while they anticommute on the same

site ($v = w$). Now, we try to determine a Hamiltonian H_Q such that, for a small a_y, the following relation holds:

$$\exp[-L(y, y+1)] = \langle y+1|(1 - a_y H_Q)|y\rangle, \tag{A 5}$$

$|y\rangle = |S_1, \ldots, S_{2N_x}\rangle$ being a product of σ_v^z eigenstates, and

$$L(y, y+1) = \beta W_1 \sum_m [u_m(y+1) - u_m(y)]^2 + \beta \sum_m f(u_{m+1}(y) - u_m(y)). \tag{A 6}$$

We observe that the whole set of states $|S_1, \ldots, S_{2N_x}\rangle$, with the prescription that the sum of S_v be zero, spans the subspace of zero total-spin z component. Considering that the value of the matrix elements of $a_y H_Q$ should be much smaller than unity, we note that, given a state for the y chain, not all the $N_s = (2N_x)!/(N_x!)^2$ chain states need to be considered for row $y+1$, but only those which are the 'leading' states in a consistent way; that is to say, on choosing an order a_y as the reference, H_Q will contain only those operators that strictly suffice to obtain the leading matrix elements (i.e. those of order a_y) correctly.

Given $|y\rangle \equiv |S_1, \ldots, S_{2N_x}\rangle$, we first consider the effect of $|y+1\rangle = |y\rangle$. In that case, $u_m(y+1) = u_m(y)$ for all m, and

$$\exp[-L(y, y+1)] = \exp\left(-\beta \sum_m f(u_{m+1}(y) - u_m(y))\right), \tag{A 7}$$

which is approximately unity (for typical $u_m(y)$ values) only if $\beta U_1 \ll 1$. Under this assumption, we can write

$$\exp[-L(y, y+1)] \approx 1 - \beta \sum_m f(u_{m+1}(y) - u_m(y)). \tag{A 8}$$

Since the constraint on $u_{m+1}(y) - u_m(y)$ has already been incorporated into the definition of the spins, the mth term under the sum on the right-hand side equals either U_1 (for $u_{m+1}(y) = u_m(y) - 1$) or zero. Then, we must count a U_1 for any $v_{m+1}(y) = v_m(y) + 1$, and a zero for $v_{m+1}(y) > v_m(y) + 1$. Accordingly, if we call $w = v_m(y)$, we have $S_{w+1} = S_w = \frac{1}{2}$ in one case, while $S_{w+1} = -S_w = -\frac{1}{2}$ in the other. As a result, we can write

$$\langle y|a_y H_Q|y\rangle = \beta U_1 \sum_v (S_v + \tfrac{1}{2})(S_{v+1} + \tfrac{1}{2}), \tag{A 9}$$

which, apart from an additive constant, can be recovered if a piece $\beta U_1 \sum_v \sigma_v^z \sigma_{v+1}^z$ is present in $a_y H_Q$.

Now suppose that the step positions at row $y+1$ differ from those at row y for one kink only. This implies that

$$\exp[-L(y, y+1)] = \exp\left(-\beta W_1 - \beta \sum_m f(u_{m+1}(y) - u_m(y))\right), \tag{A 10}$$

which is close to unity only if we assume that $\beta W_1 \gg 1$, in such a way that $\exp(-\beta W_1)$ is of order a_y (in this case, the right-hand side of equation (A 10) is almost equal to $\exp(-\beta W_1)$). An operator in H_Q which does this job is $\exp(-\beta W_1) \sum_v (\sigma_v^+ \sigma_{v+1}^- + \sigma_v^- \sigma_{v+1}^+)$.

Finally, if the states at rows y and $y+1$ were to differ by more than one spin, we would have $\exp[-L(y, y+1)] \approx \exp(-n\beta W_1)$, with a number $n > 1$ of kinks at the

yth coordinate, and this is negligible (of order a_y^n) with respect to the previous case $n = 1$. As a result, no other operator is necessary in H_Q, and its final expression is

$$a_y H_Q = -\exp(-\beta W_1) \sum_v (\sigma_v^+ \sigma_{v+1}^- + \sigma_v^- \sigma_{v+1}^+) + \beta U_1 \sum_v \sigma_v^z \sigma_{v+1}^z$$
$$= -2\exp(-\beta W_1) \sum_v (\sigma_v^x \sigma_{v+1}^x + \sigma_v^y \sigma_{v+1}^y) + \beta U_1 \sum_v \sigma_v^z \sigma_{v+1}^z \qquad \text{(A 11)}$$

with $\beta U_1 \ll 1 \ll \beta W_1$ (implying, in particular, that $W_1/U_1 \gg 1$, i.e. strong anisotropy in the VGL model).

The first term in equation (A 11) is XY like, while the other is AFM Ising like. Thus, H_Q describes a Heisenberg AFM Ising model. The character of the ground state depends on how strong βU_1 is compared with $2\exp(-\beta W_1)$. Precisely, when $J_z \equiv \beta U_1 \exp(\beta W_1)/2 > 1$, there is AFM order along z and a gap in the excitation spectrum (hence, the correlation length is finite and the vicinal is *flat*). When $J_z = 1$, the gap vanishes, and it remains zero for all $J_z < 1$. In this case, the behaviour is XY like (leading to an algebraic decay of correlations in the original model, i.e. to a *rough* vicinal). In the end, the transition temperature is given by equation (3). We note that condition (A 4) (restricting the Hilbert space of all spins σ_v to a subspace of zero total-spin z component) is a crucial requirement, since otherwise the ground-state structure is not just as indicated and, in particular, no abrupt change in behaviour will occur as a function of J_z (i.e. no phase transition in the VGL model).

Next, we include the g interaction (7). When $|y+1\rangle = |y\rangle$, we have

$$\exp[-L(y, y+1)] \approx 1 - \beta \sum_m f(u_{m+1}(y) - u_m(y)) - \beta \sum_m g(u_{m+2}(y) - u_m(y)), \qquad \text{(A 12)}$$

with both $\beta U_1 \ll 1$ and $\beta U_3 \ll 1$. Observe that $g(u_{m+2}(y) - u_m(y)) = U_3$ only when $u_{m+2}(y) = u_m(y) - 2$, or $v_{m+2}(y) = v_m(y) + 2$ (which also implies that $v_{m+1}(y) = v_m(y) + 1$). This means that, if $w = v_m(y)$, three consecutive spins are equal, $S_w = S_{w+1} = S_{w+2} = \frac{1}{2}$, and

$$\sum_m g[u_{m+2}(y) - u_m(y)] = U_3 \sum_v (S_v + \tfrac{1}{2})(S_{v+1} + \tfrac{1}{2})(S_{v+2} + \tfrac{1}{2})$$
$$= U_3 \sum_v (S_v S_{v+1} S_{v+2} + S_v S_{v+1} + \tfrac{1}{2} S_v S_{v+2})$$
$$+ \text{constant}. \qquad \text{(A 13)}$$

When $|y+1\rangle$ and $|y\rangle$ differ by one kink only, the treatment is exactly the same as before. Hence, the final Hamiltonian is

$$H_Q = -\sum_v (\sigma_v^x \sigma_{v+1}^x + \sigma_v^y \sigma_{v+1}^y) + \frac{\beta(U_1 + U_3)}{2} \exp(\beta W_1) \sum_v \sigma_v^z \sigma_{v+1}^z$$
$$+ \frac{\beta U_3}{4} \exp(\beta W_1) \sum_v \sigma_v^z \sigma_{v+2}^z + \frac{\beta U_3}{4} \exp(\beta W_1) \sum_v \sigma_v^z \sigma_{v+1}^z \sigma_{v+2}^z. \qquad \text{(A 14)}$$

H_Q can be also written in an equivalent form, in terms of spinless fermions, by performing a Jordan–Wigner transformation (which changes hard-core boson operators into anticommuting fermion operators c_v and $c_v^\dagger$) (Fradkin 1991):

$$\sigma_v^z = c_v^\dagger c_v - \tfrac{1}{2}, \sigma_v^+ = c_v^\dagger \exp\left(\mathrm{i}\pi \sum_{w<v} c_w^\dagger c_w\right), \tag{A 15}$$

which leads eventually to

$$H_Q = -\tfrac{1}{2}\sum_{v=1}^{2N_x}(c_v^\dagger c_{v+1} + c_{v+1}^\dagger c_v) + \frac{\beta U_1}{2}\exp(\beta W_1)\sum_{v=1}^{2N_x}\left(n_v n_{v+1} + \frac{U_3}{U_1} n_v n_{v+1} n_{v+2}\right), \tag{A 16}$$

with $n_v = c_v^\dagger c_v$, and where a constant and another term proportional to the total fermion number has been discarded. Note that in terms of spinless-fermion operators, equation (A 4) is a half-filling condition for the ground state, that is $\sum_v c_v^\dagger c_v = N_x$. A variational estimate of the ground-state energy of the Hamiltonian (A 16), as a function of both J_z and U_3/U_1, and hence a mean-field free energy for the extended VGL model, is derived in the following appendix.

APPENDIX B

Mapping on a quantum spin chain: variational ground states

In this appendix, we derive an expression for the average of the Hamiltonian (8) over the variational ground states representing an OF phase and a DOF phase respectively. As explained in the main text, the quantum states that correspond to the two competing flat phases have the form of a site-centred and a bond-centred CDW respectively. In order to define these states, we need to modify only slightly the standard 1D tight-binding Hamiltonian, to allow for a two-site periodicity of the number operator in the ground state at half filling. Let the 1D lattice have an even number N of sites and periodic conditions at the boundary. Then, the following trial Hamiltonians are considered (for positive t and U values):

$$H_S = -t\sum_n (c_n^\dagger c_{n+1} + c_{n+1}^\dagger c_n) + U\sum_n (-1)^n c_n^\dagger c_n, \tag{B 1}$$

where the energy is lower for occupied odd sites and unoccupied even sites, and

$$H_B = -t\sum_n (c_n^\dagger c_{n+1} + c_{n+1}^\dagger c_n) + U\sum_n (-1)^n (c_n^\dagger c_{n+1} + c_{n+1}^\dagger c_n), \tag{B 2}$$

where a lower energy is associated with the charge being concentrated on the bonds $(2m-1, 2m)$, for $m = 1, 2, \ldots$.

We first consider H_S. All the eigenvalues can be obtained by Fourier transforming the fermion operators. Call a the lattice spacing and BZ the Brillouin zone $[-\pi/a, \pi/a]$. The use of PBCs fixes the k values, which are $2\pi n/(Na) - \pi/a$, for $n = 1, 2, \ldots, N$. For simplicity, we use the same symbols for the operators and their Fourier 'coefficients', defined by

$$c_n = \frac{1}{N^{1/2}}\sum_{k\in \mathrm{BZ}} c_k \exp(\mathrm{i}kna). \tag{B 3}$$

It is worth noting that c_k and $c_k^\dagger$ obey the same anticommutation rules as the original operators. After introducing the magnetic (reduced) Brillouin zone (MBZ), $[-\pi/2a, \pi/2a]$, we eventually end up with

$$H_S = \sum_{k\in \mathrm{MBZ}} \epsilon_k (c_k^\dagger c_k - d_k^\dagger d_k) + U \sum_{k\in \mathrm{MBZ}} (c_k^\dagger d_k + d_k^\dagger c_k), \tag{B 4}$$

where $d_k = c_{k+\pi/a}$ for any $k \in$ MBZ, and $\epsilon_k = -2t\cos(ka)$. By the rotation

$$\begin{pmatrix} c_k \\ d_k \end{pmatrix} = \begin{pmatrix} \cos\theta_k & -\sin\theta_k \\ \sin\theta_k & \cos\theta_k \end{pmatrix} \begin{pmatrix} a_k \\ b_k \end{pmatrix}, \tag{B 5}$$

with $\tan(2\theta_k) = U/\epsilon_k < 0$, H_S is eventually transformed to $\sum_k E_k(a_k^\dagger a_k - b_k^\dagger b_k)$, where a_k and b_k still behave as fermion operators, and $E_k = (\epsilon_k^2 + U^2)^{1/2}$, so that the ground state is

$$|0\rangle = \prod_{|k|\leqslant k_F} b_k^\dagger |\rangle, \tag{B 6}$$

$|\rangle$ being the vacuum state and k_F determined from the lattice occupancy. For a total number $N/2$ of fermions, the Fermi sea is obtained by filling all the states of negative energy up to $k_F = \pi/2a$, the magnitude of the zone boundary vector. We note that, if θ_k is chosen between $\pi/4$ and $\pi/2$, then $\sin(2\theta_k) = U/E_k > 0$ and $\cos(2\theta_k) = \epsilon_k/E_k < 0$. This in turn determines $b_k^\dagger$:

$$b_k^\dagger = -\sin\theta_k\, c_k^\dagger + \cos\theta_k\, d_k^\dagger, \tag{B 7}$$

with $\sin\theta_k = U/[2E_k(E_k+\epsilon_k)]^{1/2}$ and $\cos\theta_k = U/[2E_k(E_k-\epsilon_k)]^{1/2}$.

Next, we consider H_B. By the same Fourier transformation (B 3), we obtain

$$H_B = \sum_{k\in \mathrm{MBZ}} \epsilon_k (c_k^\dagger c_k - d_k^\dagger d_k) - 2\mathrm{i}U \sum_{k\in \mathrm{MBZ}} \sin(ka)(c_k^\dagger d_k - d_k^\dagger c_k), \tag{B 8}$$

which can be diagonalized through the unitary transformation

$$\begin{pmatrix} c_k \\ d_k \end{pmatrix} = \begin{pmatrix} \cos\theta_k & \mathrm{i}\sin\theta_k \\ \mathrm{i}\sin\theta_k & \cos\theta_k \end{pmatrix} \begin{pmatrix} a_k \\ b_k \end{pmatrix} \quad \text{for } k > 0, \tag{B 9}$$

and

$$\begin{pmatrix} c_k \\ d_k \end{pmatrix} = \begin{pmatrix} -\cos\theta_k & -\mathrm{i}\sin\theta_k \\ \mathrm{i}\sin\theta_k & \cos\theta_k \end{pmatrix} \begin{pmatrix} a_k \\ b_k \end{pmatrix} \quad \text{for } k < 0, \tag{B 10}$$

where

$$\sin\theta_k = \frac{2U|\sin(ka)|}{[2\tilde{E}_k(\tilde{E}_k+\epsilon_k)]^{1/2}}, \cos\theta_k = \frac{2U|\sin(ka)|}{[2\tilde{E}_k(\tilde{E}_k-\epsilon_k)]^{1/2}} \tag{B 11}$$

for any $k \in$ MBZ, and $\tilde{E}_k = [\epsilon_k^2 + 4U^2\sin^2(ka)]^{1/2}$. The Hamiltonian H_B is then rewritten as $\sum_k \tilde{E}_k(a_k^\dagger a_k - b_k^\dagger b_k)$ and the ground state still has the form (B 6) (but with a different expression for $b_k^\dagger$ in terms of $c_k^\dagger$ and $d_k^\dagger$).

Once the ground state has been obtained, and c_n has been expressed in terms of c_k and d_k operators, that is

$$c_n = \frac{1}{N^{1/2}} \sum_{k\in \mathrm{MBZ}} [c_k + (-1)^n d_k] \exp(\mathrm{i}kna), \tag{B 12}$$

it remains to evaluate the ground-state average of the Hamiltonian (8). It is also convenient to express $b_k^\dagger$ in terms of $c_k^\dagger$ and $d_k^\dagger$ (the exact relationship depending on the trial Hamiltonian being used, and for H_B also on the sign of k). After rather

lengthy calculations, which we do not reproduce here, we arrive (in the thermodynamic limit) at the following results:

(i) *Site-centred CDW* (Hamiltonian H_S):

$$\begin{aligned}\langle 0|c_n^\dagger c_n|0\rangle &= \frac{1}{N}\sum_{k\in \mathrm{MBZ}} [1-(-1)^n \sin(2\theta_k)] \\ &= \tfrac{1}{2} - (-1)^n \frac{U}{\pi(1+U^2)^{1/2}} F(\kappa) \\ &\equiv \tfrac{1}{2} + (-1)^n f_S(U), \end{aligned} \tag{B 13}$$

$$\begin{aligned}\langle 0|c_n^\dagger c_{n+1}|0\rangle &= -\frac{1}{N}\sum_{k\in \mathrm{MBZ}} \cos(ka)\cos(2\theta_k) \\ &= \frac{(1+U^2)^{1/2}}{\pi} E(\kappa) - \frac{U^2}{\pi(1+U^2)^{1/2}} F(\kappa) \\ &\equiv g_S(U), \end{aligned} \tag{B 14}$$

$$\begin{aligned}\langle 0|c_n^\dagger c_{n+2}|0\rangle &= \frac{1}{N}\sum_{k\in \mathrm{MBZ}} \cos(2ka)[1-(-1)^n \sin(2\theta_k)] \\ &= (-1)^n \left[-\frac{2U(1+U^2)^{1/2}}{\pi} E(\kappa) + \frac{U(1+2U^2)}{\pi(1+U^2)^{1/2}} F(\kappa) \right] \\ &\equiv (-1)^n h_S(U), \end{aligned} \tag{B 15}$$

where $\kappa^{-2} = 1 + U^2$ and where

$$E(\kappa) = \int_0^{\pi/2} \mathrm{d}t\, (1-\kappa^2 \sin^2 t)^{1/2} \tag{B 16}$$

and

$$F(\kappa) = \int_0^{\pi/2} \mathrm{d}t\, \frac{1}{(1-\kappa^2 \sin^2 t)^{1/2}} \tag{B 17}$$

are the complete elliptic integrals of the second and first kind respectively.

(ii) *Bond-centred CDW* (Hamiltonian H_B)

$$\langle 0|c_n^\dagger c_n|0\rangle = \tfrac{1}{2}, \tag{B 18}$$

$$\begin{aligned}\langle 0|c_n^\dagger c_{n+1}|0\rangle &= -\frac{1}{N}\sum_{k\in \mathrm{MBZ}} \left(\cos(ka)\cos(2\theta_k) + (-1)^n \frac{2U\sin^2(ka)}{E_k} \right) \\ &= f_B(U) + (-1)^n g_B(U), \end{aligned} \tag{B 19}$$

$$\langle 0|c_n^\dagger c_{n+2}|0\rangle = 0, \tag{B 20}$$

where

$$f_{\mathrm{B}}(U) = \begin{cases} \dfrac{1}{\pi(1-4U^2)}\,[E(\kappa) - 4U^2 F(\kappa)] & \text{for } U < \tfrac{1}{2}, \\ \tfrac{1}{4} & \text{for } U = \tfrac{1}{2}, \\ -\dfrac{(1+p^2)^{1/2}}{\pi p^2}\left[E\left(\dfrac{p}{(1+p^2)^{1/2}}\right) - F\left(\dfrac{p}{(1+p^2)^{1/2}}\right)\right] & \text{for } U > \tfrac{1}{2}, \end{cases} \tag{B 21}$$

and

$$g_{\mathrm{B}}(U) = \begin{cases} \dfrac{2U}{\pi(1-4U^2)}\,[E(\kappa) - F(\kappa)] & \text{for } U < \tfrac{1}{2}, \\ -\dfrac{U}{2} & \text{for } U = \tfrac{1}{2}, \\ -\dfrac{2U(1+p^2)^{1/2}}{\pi p^2}\left[E\left(\dfrac{p}{(1+p^2)^{1/2}}\right) - \dfrac{1}{1+p^2}\,F\left(\dfrac{p}{(1+p^2)^{1/2}}\right)\right] & \text{for } U > \tfrac{1}{2} \end{cases} \tag{B 22}$$

for $\kappa^2 = -p^2 = 1 - 4U^2$.

Since the ground state is a Slater determinant, more complicate averages such as those of $c_n^\dagger c_n c_{n+1}^\dagger c_{n+1}$ and of $c_n^\dagger c_n c_{n+1}^\dagger c_{n+1} c_{n+2}^\dagger c_{n+2}$ can be expressed in terms of products and sums of the few averages listed above. In the end, the following expressions for the ground state averages $E_{\mathrm{S}}(U)$ and $E_{\mathrm{B}}(U)$ of the Hamiltonian (8) are obtained:

$$\frac{E_{\mathrm{S}}(U)}{N} = J_z\left[\left(1+\frac{U_3}{2U_1}\right)[\tfrac{1}{4} - f_{\mathrm{S}}^2(U)] - \left(1+\frac{U_3}{U_1}\right)g_{\mathrm{S}}^2(U) - \frac{U_3}{2U_1}\,h_{\mathrm{S}}^2(U)\right] - g_{\mathrm{S}}(U), \tag{B 23}$$

$$\frac{E_{\mathrm{B}}(U)}{N} = J_z\left[\frac{1}{4}\left(1+\frac{U_3}{2U_1}\right) - \left(1+\frac{U_3}{U_1}\right)[f_{\mathrm{B}}^2(U) + g_{\mathrm{B}}^2(U)]\right] - f_{\mathrm{B}}(U). \tag{B 24}$$

We further note that the original VGL model corresponds to $U_3 = 0$, while the XY estimate of the ground-state energy of equation (8) is obtained for $U = 0$. The latter would correspond, in surface language, to the mean-field free energy of the rough phase.

APPENDIX C

Kink correlations at roughening

We here provide the details of the very concise argument used by Den Nijs *et al.* (1985) and by Conrad *et al.* (1986) in order to justify the general expectation of a universal $2/\pi^2$ amplitude for the correlation function (4) at roughening, that is the same as in the discrete Gaussian SOS model. At first, it might not seem obvious why, near T_{R}, one may disregard the asymmetry in the step–step interaction (2) and

replace it with a symmetric square term $U_1(\Delta u)^2$, as done by Villain *et al.* (1985). However, as typical Δu values remain close to zero, the Gaussian approximation is good. This is obvious in a simulation, where conservation of the step number in the lattice sample always makes $\Delta u \approx 0$.

The main tool used by Den Nijs *et al.* (1985) is the Poisson summation formula, which allows one to convert a sum over discrete heights into an integral over field variables. In particular, the partition function of a general discrete SOS model $H_{\mathrm{SOS}} = \sum_{x,y} V(\phi_x - \phi_y; x - y)$, with integer heights ϕ_x defined over a two-dimensional (2D) regular lattice of x sites, can be rearranged as follows (Chui and Weeks 1976):

$$Z_{\mathrm{SOS}} = \int \mathcal{D}\phi \exp\left(-\beta \sum_{x,y} V(\phi_x - \phi_y; x - y)\right) \prod_x \sum_{N_x=-\infty}^{+\infty} \exp(2\pi \mathrm{i} N_x \phi_x), \quad \text{(C 1)}$$

with real ϕ_x variables. The sine–Gordon partition function follows by inserting a small positive power-counting fugacity factor into the sum:

$$Z'_{\mathrm{SOS}} = \int \mathcal{D}\phi \exp\left(-\beta \sum_{x,y} V(\phi_x - \phi_y; x - y)\right) \prod_x \sum_{N_x=-\infty}^{+\infty} z^{N_x^2} \exp(2\pi \mathrm{i} N_x \phi_x), \quad \text{(C 2)}$$

or, in an equivalent way,

$$Z_{\mathrm{sG}} = \int \mathcal{D}\phi \exp\left[-\beta \sum_{x,y} V(\phi_x - \phi_y; x - y) + \sum_x \sum_{N=1}^{\infty} 2 z_N \cos(2\pi N \phi_x)\right], \quad \text{(C 3)}$$

where z_N is assumed to be small for any N. If $z_1 > 0$ at any temperature, which corresponds to the no-PR case, the roughening behaviour of model (C 3) is only controlled by the first term $N = 1$ in the sum.

For bipartite lattices, as in the body-centred case, the only change to be made in the above equation (C 1) is in the way that the constraint on the height values is incorporated into the functional integral (whereas any possible restriction on the difference between nearest-neighbour heights is accounted for by the potential V). In the particular case of a bcc metal (001) surface, it is convenient to assign integer heights to integer sites (i.e. lattice sites having integer x and y coordinates) and half-integer heights to half-integer sites (the horizontal lattice spacing is $a = 1$). Then, the measure or weight function which takes care of the (vertical) constraints will be

$$W[\phi] = \prod_x^{(A)} \sum_{n_x=-\infty}^{+\infty} \delta\left(\frac{\phi_x}{a_z} - n_x\right) \times \prod_x^{(B)} \sum_{n_x=-\infty}^{+\infty} \delta\left(\frac{\phi_x}{a_z} - (n_x + \tfrac{1}{2})\right), \quad \text{(C 4)}$$

where a_z is the difference between two consecutive height values in a column, and A and B are the square sublattices of integer and half-integer sites respectively. By use of the Poisson formula, and noting that $\exp(2\pi \mathrm{i} N_x x_x / a)$ is 1 for $x \in A$ and $(-1)^{N_x}$ for $x \in B$, we also have

$$W[\phi] = \prod_x \sum_{N_x=-\infty}^{+\infty} \exp\left[2\pi \mathrm{i} N_x \left(\frac{\phi_x}{a_z} + \frac{x_x}{a}\right)\right]. \quad \text{(C 5)}$$

The sine–Gordon problem peculiar to body-centred SOS roughening, in that it belongs to the same universality class, is then

$$Z_{\mathrm{sG}} = \int \mathcal{D}\phi \exp\left\{ \sum_{\langle x,y \rangle} K \frac{(\phi_x - \phi_y)^2}{a_z^2} + \sum_x \sum_{N=1}^{\infty} 2z_N \cos\left[2\pi N \left(\frac{\phi_x}{a_z} + \frac{x_x}{a} \right) \right] \right\}. \quad \text{(C 6)}$$

At roughening, the height–height correlation function would behave, according to renormalization group theory, as

$$\frac{\langle (\phi_x - \phi_y)^2 \rangle}{a_z^2} \sim \frac{X_1}{\pi^2} \ln\left(\frac{|x-y|}{a_z} \right), \quad \text{(C 7)}$$

with a roughness parameter X_1 equal to $2/N_*^2$, N_* being the smallest wave-vector in equation (C 6) for which the operator $\exp(2\pi \mathrm{i} N x_x/a)$ is not modulated at any of the lattice sites, that is to say, is 1 at any x (Den Nijs *et al.* 1985). It is obvious that $N_* = 2$; hence the critical amplitude $2/\pi^2$ follows by noting that the difference between two nearest-neighbour heights is $a_z/2$.

We now turn to the fcc metal (115) surface case. Let a SOS condition be still assumed along [001] and call a the nearest-neighbour distance in the fcc lattice, as usual. If we imagine that all the three-dimensional fcc lattice sites are projected along the [55$\bar{2}$] direction (i.e. in such a way that the heights ϕ of two consecutive atoms in a column will differ by $a2^{1/2}\cos\alpha$ after projection, with $\cos\alpha = 5 \times 3^{1/2}/9$), then five different categories of sites (from A to E) can be identified in the x–y plane, according to the criterion that two sites are in the same class if their x coordinates differ by $\frac{5}{2}a$. Calling ϕ' the projected heights, the weight function can thus be written as

$$\begin{aligned} W[\phi] &= \prod_x^{(\mathrm{A})} \sum_{n_x=-\infty}^{+\infty} \delta\left(\frac{\phi'_x}{a2^{1/2}\cos\alpha} - n_x \right) \times \prod_x^{(\mathrm{B})} \sum_{n_x=-\infty}^{+\infty} \delta\left(\frac{\phi'_x}{a2^{1/2}\cos\alpha} - (n_x + \tfrac{1}{5}) \right) \\ &\quad \times \cdots \times \prod_x^{(\mathrm{E})} \sum_{n_x=-\infty}^{+\infty} \delta\left(\frac{\phi'_x}{a2^{1/2}\cos\alpha} - (n_x + \tfrac{4}{5}) \right) \\ &= \prod_x^{(\mathrm{A})} \sum_{N_x=-\infty}^{+\infty} \exp\left(2\pi \mathrm{i} N_x \frac{\phi'_x}{a2^{1/2}\cos\alpha} \right) \\ &\quad \times \prod_x^{(\mathrm{B})} \sum_{N_x=-\infty}^{+\infty} \exp\left(-\frac{2\pi}{5} \mathrm{i} N_x \right) \exp\left(2\pi \mathrm{i} N_x \frac{\phi'_x}{a2^{1/2}\cos\alpha} \right) \\ &\quad \times \cdots \times \prod_x^{(\mathrm{E})} \sum_{N_x=-\infty}^{+\infty} \exp\left(-\frac{8\pi}{5} \mathrm{i} N_x \right) \exp\left(2\pi \mathrm{i} N_x \frac{\phi'_x}{a2^{1/2}\cos\alpha} \right), \end{aligned} \quad \text{(C 8)}$$

where in the last step the Poisson formula has been used. Now, the following association is decided: we put into class $A, B, \ldots, E$ all the sites with $x_x = 0 + k\frac{5}{2}a, a + k\frac{5}{2}a, \ldots, 4a + k\frac{5}{2}a$, k integer. Then, the weight function can be written in the more compact form

$$W[\phi] = \prod_x \sum_{N_x=-\infty}^{+\infty} \exp\left[2\pi \mathrm{i} N_x \left(\frac{\phi'_x}{a2^{1/2}\cos\alpha} - \frac{6}{5}\frac{x_x}{a} \right) \right]. \quad \text{(C 9)}$$

What remains to be found is a proper Gaussian term in the sine–Gordon Hamiltonian which is a function of ϕ' variables only. In order to accomplish this task, we observe that the following relation holds:

$$\phi_x - \phi_y + (x_x - x_y)\tan\alpha = \frac{\phi'_x - \phi'_y}{\cos\alpha}, \tag{C 10}$$

as obtained from the equations which transform the ϕ_x into ϕ'_x variables (i.e. a combination of a translation and a rotation of α°). In particular, the left-hand side of equation (C 10) is the usual squared height difference after a trivial term due to the average inclination of the vicinal on the x–y plane has been subtracted. In particular, equation (C 10) suggests the following sine–Gordon model as appropriate to the roughening of the vicinal:

$$Z_{\mathrm{sG}} = \int \mathcal{D}\phi' \exp\left\{ \sum_{\langle x,y\rangle} K \frac{(\phi_x - \phi'_y)^2}{2a^2\cos^2\alpha} + \sum_x \sum_{N=1}^{\infty} 2z_N \cos\left[2\pi N\left(\frac{\phi'_x}{a2^{1/2}\cos\alpha} - \frac{6}{5}\frac{x_x}{a}\right)\right]\right\}, \tag{C 11}$$

where the denominator in the Gaussian part is the square of the distance, along [115], between two atoms that are consecutive in a column (see also equation (C 6), where a similar choice was made). At the roughening transition of the [115] facet, we should then have

$$\frac{\langle(\phi'_x - \phi'_y)^2\rangle}{2a^2\cos^2\alpha} \sim \frac{X_1}{\pi^2}\ln\left(\frac{|x-y|}{a}\right), \tag{C 12}$$

with $X_1 = 2/N_*^2$, $N_* = 5$ now being the smallest wave-vector in equation (C 11) for which the sine–Gordon operator $\exp(2\pi \mathrm{i} N \frac{6}{5} x_x/a)$ equals unity at any site. Equation (C 12) is the same as equation (1) of Den Nijs *et al.* (1985).

Finally, suppose that x and y correspond to step atoms, that is let ϕ be higher at $x(y)$ than at the next site on the right. In this case, x has a u_x associated with it, and the same occurs for y. Since

$$u_x - u_y = \frac{\phi'_x - \phi'_y}{a\sin\alpha}, \tag{C 13}$$

use of equation (C 12) leads to the expected behaviour of the kink–kink correlation function at roughening:

$$\langle(u_x - u_y)^2\rangle \sim \frac{2}{\pi^2}\ln\left(\frac{|x-y|}{a}\right), \tag{C 14}$$

a result which in fact holds identically for all the $(1, 1, 2n+1)$ vicinals (for the general proof, it suffices to take $\tan\alpha_{2n+1} = 2^{1/2}/(2n+1)$).

In closing this section, we briefly comment on the experimental determination of the roughening temperature by X-ray or atom scattering. In the single-atom scattering approximation, the scattered beam intensity is given by

$$\begin{aligned} I(\mathbf{Q}, q_\perp) &\propto \left\langle \left| \sum_x \exp\left[\mathrm{i}(\mathbf{Q}\cdot x + q_\perp \phi'_x)\right] \right|^2 \right\rangle \\ &= \sum_{x,y} \exp\left[\mathrm{i}\mathbf{Q}\cdot(x-y)\right]\langle \exp\left[\mathrm{i}q_\perp(\phi'_x - \phi'_y)\right]\rangle, \end{aligned} \tag{C 15}$$

where $\mathbf{Q}$ (a 2D vector) and $q_\perp$ are the component of the momentum transfer in the substrate plane and along [115] respectively. Making a Gaussian *Ansatz* for the distribution of heights, we obtain

$$\langle \exp [iq_\perp(\phi'_x - \phi'_y)] \rangle \approx \exp [-\tfrac{1}{2} q_\perp^2 \langle (\phi'_x - \phi'_y)^2 \rangle], \tag{C 16}$$

which in the rough phase and in antiphase conditions (which for a vicinal is $q_\perp = \pi/c$ for $c = a \sin \alpha$) simplifies to $(|x-y|/a)^{-\tau}$ when $|x-y| \gg a$, where $\tau = 1$ for $T = T_R$ and $\tau > 1$ for $T > T_R$. A similar behaviour would also occur at T_{PR}, but with a non-universal $\tau < 1$. From the large-distance behaviour of the average (C 16), it then follows (Lapujoulade and Salanon 1992) that the total Bragg intensity vanishes in antiphase for all $T \geqslant T_R$, and also for $T = T_{PR}$. Conversely, in a flat surface (either ordered or disordered), large-distance saturation of $G(m)$ implies delta Bragg peaks at any $q_\perp$, $I(\mathbf{G}, q_\perp) \propto \delta_{\mathbf{Q},\mathbf{G}}$, and hence a non-zero total Bragg intensity in antiphase for both $T < T_{PR}$ and $T_{PR} < T < T_R$. In conclusion, PR of a vicinal can in principle be detected from the behaviour of the coherent (Bragg) intensity in antiphase as a function of temperature, its fingerprint being a decrease (at T_{PR}), followed by a recovery (in the DOF phase), and eventually by another decrease (at the entrance of the rough phase).

APPENDIX D

Kink statistics at low temperatures

In this appendix, the problem of the distribution of kinks in a primary step at low temperatures is considered.

Let the temperature be low compared with the roughening temperature T_R. Then, to a good approximation, the statistics of kinks can be computed by assuming that a step can only make small lateral excursions from its equilibrium position, both on the left and on the right, while the neighbouring steps are fixed and straight (Bartelt *et al.* 1990; Sanders and Frenken 1992). In this case, the kink Hamiltonian which more naturally represents the low-temperature behaviour of model (5) is

$$H = W_1 \sum_{y=1}^{N_y} \delta(|u_y - u_{y+1}| - 1) + W_2 \sum_{y=1}^{N_y} \delta(|u_y - u_{y+2}| - 2) + 2U_1 \sum_{y=1}^{N_y} u_y^2, \tag{D 1}$$

with $u_y = -1, 0, 1$ and $u_{y+1} - u_y = 0, \pm 1$. This 1D model can be treated in an exact way by the transfer-matrix method. A pair of consecutive step sites is the elementary lattice unit; it can be in any of seven states. In the thermodynamic limit, the exact free energy per site is equal to $f = -\frac{1}{2} k_B T \ln \lambda_1$, where λ_1 is the maximum eigenvalue of the transfer matrix. Thermal averages of interest are the fraction of step sites which are not in the equilibrium position given by

$$\frac{1}{N_y} \left\langle \sum_y u_y^2 \right\rangle = \frac{1}{2} \left(\frac{\partial \beta f}{\partial \beta U_1} \right)_{\beta W_1, \beta W_2}, \tag{D 2}$$

the density of kinks given by

$$\frac{1}{N_y} \left\langle \sum_y \delta(|u_y - u_{y+1}| - 1) \right\rangle = \left(\frac{\partial \beta f}{\partial \beta W_1} \right)_{\beta W_2, \beta U_1}, \tag{D 3}$$

and the density of bound pairs of parallel kinks given by

$$\frac{1}{N_y}\left\langle \sum_y \delta(|u_y - u_{y+2}| - 2) \right\rangle = \left(\frac{\partial \beta f}{\partial \beta W_2}\right)_{\beta W_1, \beta U_1} \tag{D 4}$$

In principle, a low-temperature measurement of these three quantities will enable us to obtain the values of W_1, W_2 and U_1. However, since in practice the ratio of W_1 to U_1 is very large, the density of kinks is so low that an accurate estimate of the couplings from the experiment is not possible.

We see here how to express the same averages in equations (D 2), (D 3) and (D 4) in a matrix form. Following Sanders and Frenken (1992), the step itself can be viewed as a Markov chain, in that the probability of observing a pair of consecutive sites $(2k+1, 2k+2)$ in a certain state S_{k+1} (with $k = 1, 2, \ldots$), on condition that the pairs labelled $1, 2, \ldots, k$ are in states $S_1, S_2, \ldots, S_k$, only depends on S_k (in the thermodynamic limit), and not on the states of other pairs. Precisely, this conditional or transition probability is

$$P(S_{k+1}|S_1, \ldots, S_k) = T_{S_k, S_{k+1}} \frac{v_{S_{k+1}}}{\lambda_1 v_{S_k}} \equiv P_{S_k, S_{k+1}}, \tag{D 5}$$

$T_{m,n}$ being the transfer matrix ($m, n = 1, \ldots, 7$ are labels of pair states) and v_m the mth component of the leading T eigenvector (which is real and positive according to the Perron–Frobenius theorem, notwithstanding the fact that T is not symmetric). From equation (D 5), it is clear that $P_{m,n}$ is a stochastic matrix. Moreover, the (unconditional) probability that a given pair of consecutive step sites is in state m obeys $P_m = \sum_{n=1}^{7} P_n P_{n,m}$. Together with $\sum_{m=1}^{7} P_m = 1$, the P_m are easily determined, for example by Gaussian elimination. Once the P_m are known, the probability weight of any local kink configuration can be easily calculated, including the averages at equations (D 2), (D 3) and (D 4). Using obvious symmetry considerations, we have

$$\langle u_y^2 \rangle = P_{(-1,-1)} + P_{(-1,0)} + P_{(1,0)} + P_{(1,1)}, \tag{D 6}$$

$$\langle \delta(|u_y - u_{y+1}| - 1) \rangle = P_{(-1,0)} + P_{(0,-1)} + P_{(0,1)} + P_{(1,0)}, \tag{D 7}$$

$$\begin{aligned} \langle \delta(|u_y - u_{y+2}| - 2) \rangle = {} & P_{(-1,0)}(P_{(-1,0),(1,0)} + P_{(-1,0),(1,1)}) \\ & + P_{(1,0)}(P_{(1,0),(-1,-1)} + P_{(1,0),(-1,0)}). \end{aligned} \tag{D 8}$$

We have verified that, for $W_2 = 2W_1 = 40U_1$, the expressions above give exactly the same results as determined from the numerical derivatives of the free energy (figure D 1(a)).

Once a Markov property has been recognized in the way that kinks are distributed along the step, it is not difficult to calculate other quantities which are more representative of the correlations between the kinks. For instance, given a direction along the step, we may ask what is the probability $\Pi(d)$ that, starting with a kink at a certain site, the next kink (parallel or not) first occurs d sites after. The following expression for $\Pi(d)$ holds:

$$\begin{aligned}
\Pi(1) &= P_{(-1,0)}(P_{(-1,0),(-1,-1)} + P_{(-1,0),(-1,0)} + P_{(-1,0),(1,0)} + P_{(-1,0),(1,1)}) \\
&\quad + P_{(0,-1)}(P_{(0,-1),(0,-1)} + P_{(0,-1),(0,0)} + P_{(0,-1),(0,1)}) \\
&\quad + P_{(0,1)}(P_{(0,1),(0,-1)} + P_{(0,1),(0,0)} + P_{(0,1),(0,1)}) \\
&\quad + P_{(1,0)}(P_{(1,0),(-1,-1)} + P_{(1,0),(-1,0)} + P_{(1,0),(1,0)} + P_{(1,0),(1,1)}), \\
\Pi(2n+1) &= P_{(-1,0)}P_{(-1,0),(0,0)}P^{n-1}_{(0,0),(0,0)} \\
&\quad \times (P_{(0,0),(-1,-1)} + P_{(0,0),(-1,0)} + P_{(0,0),(1,0)} + P_{(0,0),(1,1)}) \\
&\quad + P_{(0,-1)}P_{(0,-1),(-1,-1)}P^{n-1}_{(-1,-1),(-1,-1)} \\
&\quad \times (P_{(-1,-1),(0,-1)} + P_{(-1,-1),(0,0)} + P_{(-1,-1),(0,1)}) \\
&\quad + P_{(0,1)}P_{(0,1),(1,1)}P^{n-1}_{(1,1),(1,1)}(P_{(1,1),(0,-1)} + P_{(1,1),(0,0)} + P_{(1,1),(0,1)}) \\
&\quad + P_{(1,0)}P_{(1,0),(0,0)}P^{n-1}_{(0,0),(0,0)} \\
&\quad \times (P_{(0,0),(-1,-1)} + P_{(0,0),(-1,0)} + P_{(0,0),(1,0)} + P_{(0,0),(1,1)})(n = 1, 2, \ldots),
\end{aligned} \tag{D 9}$$

and

$$\begin{aligned}
\Pi(2) &= P_{(-1,0)}(P_{(-1,0),(0,-1)} + P_{(-1,0),(0,1)}) + P_{(0,-1)}P_{(0,-1),(-1,0)} \\
&\quad + P_{(0,1)}P_{(0,1),(1,0)} + P_{(1,0)}(P_{(1,0),(0,-1)} + P_{(1,0),(0,1)}), \\
\Pi(2n) &= P_{(-1,0)}P_{(-1,0),(0,0)}P^{n-2}_{(0,0),(0,0)}(P_{(0,0),(0,-1)} + P_{(0,0),(0,1)}) \\
&\quad + P_{(0,-1)}P_{(0,-1),(-1,-1)}P^{n-2}_{(-1,-1),(-1,-1)}P_{(-1,-1),(-1,0)} \\
&\quad + P_{(0,1)}P_{(0,1),(1,1)}P^{n-2}_{(1,1),(1,1)}P_{(1,1),(1,0)} \\
&\quad + P_{(1,0)}P_{(1,0),(0,0)}P^{n-2}_{(0,0),(0,0)}(P_{(0,0),(0,-1)} + P_{(0,0),(0,1)})(n = 2, 3 \ldots).
\end{aligned} \tag{D 10}$$

In figure D 1 (*b*), the kink-to-kink separation statistics are reported for a number of βU_1 values, for $W_2 = 2W_1 = 40U_1$. The average separation between two kinks can be calculated from this as

$$\bar{d} = \frac{\sum_{n=1}^{\infty} n\Pi(n)}{\langle \delta(|u_y - u_{y+1}| - 1)\rangle}. \tag{D 11}$$

When $W_2 = +\infty$, the overall picture remains unchanged. Simply, all curves in figure D 1 become depressed as a result of the comparatively lower kink density at each temperature.

Next, we consider the kink statistics over a [$\bar{1}$10] secondary step running along the nominal step direction and thus confined between two fixed and straight primary steps. At variance with the previous case, step meandering is now restricted to *two* positions only, and the kink Hamiltonian thus is

$$H = W_1 \sum_{y=1}^{N_y} \delta(|u_y - u_{y+1}| - 1) + W_2' \sum_{y=1}^{N_y} \delta(|u_y - u_{y+1}| - 1)\delta(|u_{y+1} - u_{y+2}| - 1), \tag{D 12}$$

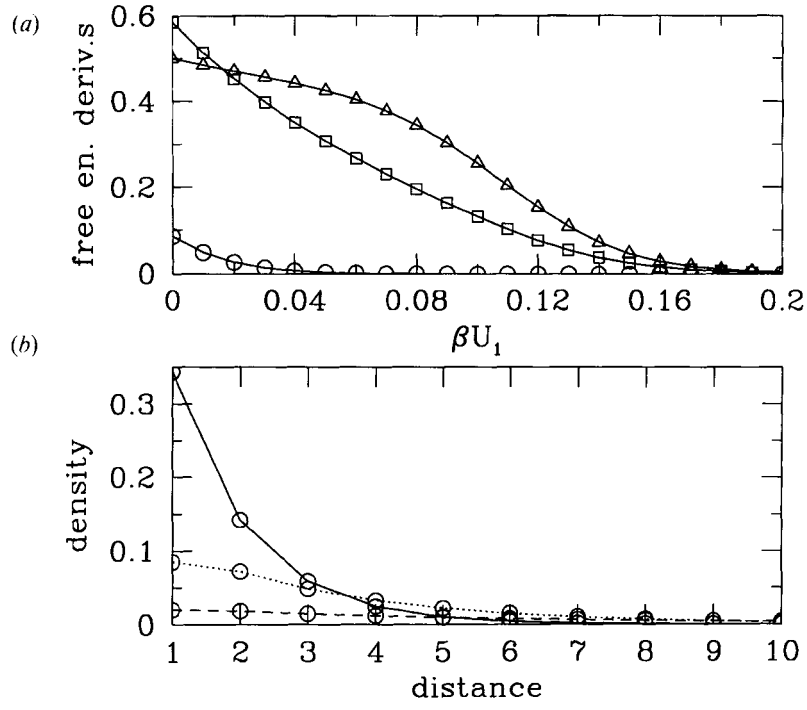

Figure D 1. Exact results for the Hamiltonian (D 1), for $W_2 = 2W_1 = 40U_1$: (*a*) the relevant thermodynamic averages of the fraction of displaced step sites (△), the kink density (□) and the density of bound pairs of parallel kinks (○); (*b*) the kink-to-kink separation statistics for selected temperature values $\beta U_1 = 0$ (——), $\beta U_1 = 0.05$ (. . . . . .) and $\beta U_1 = 0.1$ (- - -).

where for example $u_y = 0, 1$ and $W_2' > 0$ is a short-range repulsion between antiparallel kinks. The lattice unit is still represented by a pair of consecutive step sites, and the total number of states is now four. The kink density and the density of bound pairs of antiparallel kinks are given respectively by

$$\frac{1}{N_y}\left\langle \sum_y \delta(|u_y - u_{y+1}| - 1) \right\rangle = \left(\frac{\partial \beta f}{\partial \beta W_1}\right)_{\beta W_2'} = P_{(0,1)} + P_{(1,0)}, \tag{D 13}$$

$$\frac{1}{N_y}\left\langle \sum_y \delta(|u_y - u_{y+1}| - 1)\delta(|u_{y+1} - u_{y+2}| - 1) \right\rangle = \left(\frac{\partial \beta f}{\partial \beta W_2'}\right)_{\beta W_1} = P_{(0,1)}(P_{(0,1),(0,0)} + P_{(0,1),(0,1)}) + P_{(1,0)}(P_{(1,0),(1,0)} + P_{(1,0),(1,1)}). \tag{D 14}$$

We have verified (for $W_2' = 2W_1$) that the numerical derivatives of the exact free energy indeed coincide at all temperatures with the values obtained from the right-

hand side above (figure D 2 (*a*)). The probability $\Pi(d)$ of an excursion of length d is calculated accordingly as

$$\begin{aligned}\Pi(1) &= P_{(0,1)}(P_{(0,1),(0,0)} + P_{(0,1),(0,1)}) \\ &\quad + P_{(1,0)}(P_{(1,0),(1,0)} + P_{(1,0),(1,1)}), \\ \Pi(2n+1) &= P_{(0,1)}P_{(0,1),(1,1)}P^{n-1}_{(1,1),(1,1)}(P_{(1,1),(0,0)} + P_{(1,1),(0,1)}) \\ &\quad + P_{(1,0)}P_{(1,0),(0,0)}P^{n-1}_{(0,0),(0,0)}(P_{(0,0),(1,0)} + P_{(0,0),(1,1)})(n = 1, 2, \ldots),\end{aligned} \tag{D 15}$$

and

$$\begin{aligned}\Pi(2) &= P_{(0,1)}P_{(0,1),(1,0)} + P_{(1,0)}P_{(1,0),(0,1)}, \\ \Pi(2n) &= P_{(0,1)}P_{(0,1),(1,1)}P^{n-2}_{(1,1),(1,1)}P_{(1,1),(1,0)} \\ &\quad + P_{(1,0)}P_{(1,0),(0,0)}P^{n-2}_{(0,0),(0,0)}P_{(0,0),(0,1)}(n = 2, 3, \ldots).\end{aligned} \tag{D 16}$$

In figure D 2 (*b*), the density of excursions is reported for a number of βW_1 values, for $W_2' = 2W_1$.

Finally, when $W_2' = 0$, the problem (D 12) becomes equivalent to the 1D Ising model with Hamiltonian $H = W_1/2\sum_i(1 - S_iS_{i+1})$, where $S_i = -1$ (1) for

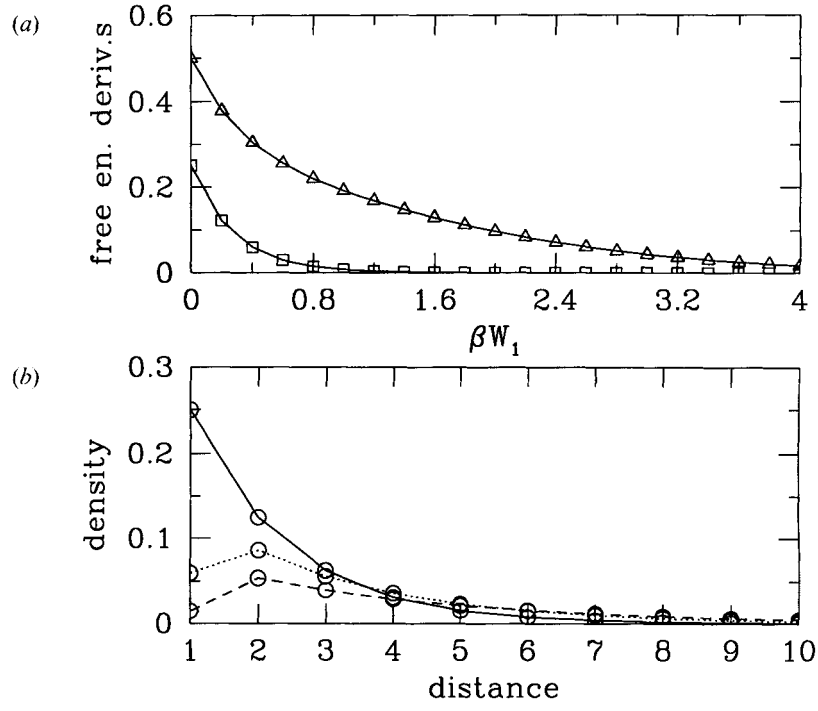

Figure D 2. Exact results for the Hamiltonian (D 12), for $W_2' = 2W_1$: (*a*) the relevant thermodynamic averages of the kink density (□) and the density of bound pairs of antiparallel kinks (△); (*b*) the kink-to-kink separation statistics for selected temperature values $\beta W_1 = 0$ (——), $\beta W_1 = 0.4$ (. . . . .) and $\beta W_1 = 0.8$ (- - -).

$u_i = 0$ (1). This is similar to the model considered by Sanders and Frenken (see equation (2.7) of Sanders and Frenken (1992) but with $\nu = \beta W_1/2$ and $L = 0$). In particular, the probability of having $S_i = \pm 1$ is $\frac{1}{2}$ in either case, while the transition probabilities are

$$P_{-1,-1} = P_{1,1} = \frac{1 + \tanh \nu}{2}, P_{-1,1} = P_{1,-1} = \frac{1 - \tanh \nu}{2}. \tag{D 17}$$

The kink density is thus equal to

$$P_{-1}P_{-1,1} + P_1 P_{1,-1} = \frac{1 - \tanh \nu}{2}$$
$$= (1 + \exp(\beta W_1))^{-1}. \tag{D 18}$$

Note that this expression is different from that obtained by Hoogeman *et al.* (1996) for the density of kinks along an *unconfined* [$\bar{1}$10] secondary step.

References

Bartelt, N. C., Einstein, T. L., and Williams, E. D., 1990, *Surf. Sci.*, **240**, L591.

Celestini, F., Passerone, D., Ercolessi, F., and Tosatti, E., 2000, *Phys. Rev. Lett.*, **84**, 2203.

Chui, S. T., and Weeks, J. D., 1976, *Phys. Rev.* B, **14**, 4978.

Conrad, E. H., Aten, R. M., Kaufman, D. S., Allen, L. R., Engel, T., Den Nijs, M., and Riedel, E. K., 1986, *J. Chem. Phys.*, **85**, 4756.

Day, P. Lysek, M., LaMadrid, M., and Goodstein, D., 1993, *Phys. Rev.* B, **47**, 10716.

Den Nijs, M., 1991, *Phase Transitions in Surface Films*, Vol. 2, edited by H. Taub *et al.* (New York: Plenum).

Den Nijs, M., Riedel, E. K., Conrad, E. H., and Engel, T., 1985, *Phys. Rev. Lett.*, **55**, 1689.

Den Nijs, M., and Rommelse, K., 1989, *Phys. Rev.* B, **40**, 4709.

Fradkin, E., 1991, *Field Theories of Condensed Matter Systems* (Redwood, California: Addison-Wesley).

Fradkin, E., and Susskind, L., 1978, *Phys. Rev.* D, **17**, 2637.

Frenken, J. W. M., and Stoltze, P., 1999, *Phys. Rev. Lett.*, **82**, 3500.

Hertz, J. A., 1976, *Phys. Rev.* B, **14**, 1165.

Hoogeman, M. S., and Frenken, J. W. M., 2000, *Surf. Sci.*, **448**, 155.

Hoogeman, M. S., Klik, M. A. J., Schlösser, D. C., Kuipers, L., and Frenken, J. W. M., 1999, *Phys. Rev. Lett.*, **82**, 1728.

Hoogeman, M. S., Schlösser, D. C., Sanders, J. B., Kuipers, L., and Frenken, J. W. M., 1996, *Phys. Rev.* B, **53**, R13299.

Jagla, E. A., Prestipino, S., and Tosatti, E., 1999, *Phys. Rev. Lett.*, **83**, 2753.

Kogut, J. B., 1979, *Rev. mod. Phys.*, **51**, 659.

Kossel, W., 1927, *Nachr. Ges. Wiss. Göttingen*, **135**.

Lapujoulade, J., and Salanon, B., 1992, *Phase Transitions in Surface Films*, Vol. 2, edited by H. Taub *et al.* (New York: Plenum).

Marchenko, V. I., and Parshin, A. Ya., 1981, *Soviet. Phys. JETP*, **52**, 129.

Prestipino, S., Santoro, G., and Tosatti, E., 1995, *Phys. Rev. Lett.*, **75**, 4468.

Prestipino, S., and Tosatti, E., 1997, *Surf. Sci.*, **377–379**, 509; 1998, *Phys. Rev.* B, **57**, 10157; 1999, *ibid*, **59**, 3108.

Rickman, J. M., and Srolovitz, D. J., 1993, *Surf. Sci.*, **284**, 211.

Sanders, J. B., and Frenken, J. W. M., 1992, *Surf. Sci.*, **275**, 142.

Santoro, G., Vendruscolo, M., Prestipino, S., and Tosatti, E., 1996, *Phys. Rev.* B, **53**, 13169.

Selke, W., and Szpilka, A. M., 1986, *Z. Phys.* B, **62**, 381.

Stranski, I. N., 1928, *Z. Phys. Chem.*, **136**, 259.

Villain, J., Grempel, D. R., and Lapujoulade, J., 1985, *J. Phys.* F, **15**, 809.

Weichman, P. B., and Prasad, A., 1996, *Phys. Rev. Lett.*, **76**, 2322.

Youn, H. S., and Hess, G. B., 1990, *Phys. Rev. Lett.*, **64**, 918.

Youn, H. S., Meng, X. F., and Hess, G. B., 1993, *Phys. Rev.* B, **48**, 14556.